NASA TECHNICAL NOTE

NASA TN D-4367

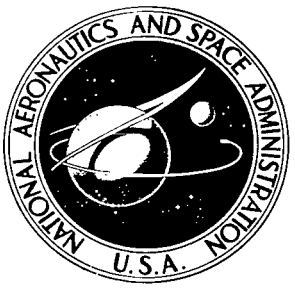

NASA TN D-4367

PRESSURE AND HEAT TRANSFER ON BLUNT CURVED PLATES WITH CONCAVE AND CONVEX SURFACES IN HYPERSONIC FLOW

by Davis H. Crawford

Langley Research Center
Langley Station, Hampton, Va.

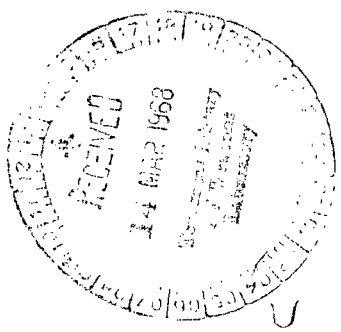

NATIONAL AERONAUTICS AND SPACE ADMINISTRATION • WASHINGTON, D. C. • MARCH 1968

PRESSURE AND HEAT TRANSFER ON BLUNT CURVED PLATES WITH CONCAVE AND CONVEX SURFACES IN HYPERSONIC FLOW

By Davis H. Crawford

Langley Research Center
Langley Station, Hampton, Va.

NATIONAL AERONAUTICS AND SPACE ADMINISTRATION

For sale by the Clearinghouse for Federal Scientific and Technical Information
Springfield, Virginia 22151 – CFSTI price $3.00

PRESSURE AND HEAT TRANSFER ON BLUNT CURVED PLATES WITH CONCAVE AND CONVEX SURFACES IN HYPERSONIC FLOW

By Davis H. Crawford
Langley Research Center

SUMMARY

Pressure and heat transfer have been measured in the presence of both favorable and adverse pressure gradients at Mach numbers of 6.8 and 9.6 and Reynolds numbers based on length from 0.5×10^6 to 3.0×10^6. The pressure data were represented by a power law relationship, and the empirical constants from this relationship were used to calculate the heat transfer by a simplified method. This method allows similar compressible solutions of the laminar boundary layer with pressure gradient to be directly applied without the use of integral or iterative methods. The results of these calculations are compared with the experimental values and with the calculated results from a more complex laminar similarity method requiring a machine program and iterative procedures. Differences between the two theoretical methods are shown to be slight for many applications. Applications where the simple method is less accurate are defined.

INTRODUCTION

Boundary-layer calculations by similarity methods are applicable with accuracy to a wide range of flow conditions where deviations from a calorically perfect gas are small. These similar solutions may be applied with good results to a diverse assortment of hydrodynamic configurations. Even when the caloric imperfections of the fluids are not small, the results of similar solutions are considered conservative when used to estimate heat transfer, displacement effects, and momentum thickness.

Similarity solutions of the boundary layer are ordinarily tabulated as functions of quantities in the transformed plane where similarity was achieved. The use of these calculations involves a thorough understanding of the derivation of the relations as well as tedious numerical operations which are best assigned to a high-speed electronic computer. Some references have reported these solutions in a form usable in a straightforward manner which circumvents the intricate digital procedure.

One such similarity method by Li and Nagamatsu presented boundary-layer calculations for hypersonic flow. (See ref. 1.) This scheme used $p \propto x^n$ and the hypersonic

approximations, $u_e \approx u_\infty$ and $1 - \frac{t_e}{t_o} \approx 1$, to simplify the boundary-layer equations in the transformed plane. The assumption of similarity, which allowed the momentum equation to be reduced to an ordinary differential equation with the independent variable η, resulted in a relation between the Falkner-Skan velocity gradient parameter β and the pressure gradient parameter n. A greatly simplified method by Bertram and Feller (ref. 2) has been advanced for laminar boundary-layer calculations which used this hypersonic relation between β and n with a different $N_{Pr} = 1$ similar compressible solution of the boundary layer to correct a suitable flat-plate solution for the effects of pressure gradient. Bertram shows that this method is inapplicable when $n < -1$, and implies that this method is of doubtful accuracy when the value of n is near -1.

Another method recently introduced by the present author (ref. 3) provides solutions of the boundary-layer equations in closed form. This method which does not involve hypersonic approximations is applicable when the pressure distribution is of the form $p \propto (x + A)^n$. Assumption of this type of pressure distribution along with a perfect gas equation of state and constant entropy at the edge of the boundary layer allowed the $N_{Pr} = 1$ compressible solutions of references 4 and 5 to be expressed directly in terms of quantities in the real plane. When the hypersonic approximations $(t_e/t_o) \to 0$ and $(t_\infty/t_o) \to 0$ are made, and when $A \to 0$, the relations of reference 3 become identical to the relations of reference 2. Comparison of values calculated by these two methods can therefore be used to determine the effect of hypersonic approximations for specific flow conditions.

In the present investigation, measured pressure and heat transfer were obtained on a two-dimensional model with a hemicylindrically blunted leading edge and one concave and one convex curved surface. The main body of the data was taken with end plates, but some data were taken without end plates to show the end-plate effect. The model was tested at $M = 6.8$ and 9.6 and at $\alpha = -8^\circ$, 0°, and 15° for both Mach numbers. The free-stream Reynolds numbers based on model length varied from 1×10^6 to 2.8×10^6 at $M = 6.8$ and from 0.6×10^6 to 1×10^6 at $M = 9.6$. Therefore, laminar flow conditions occurred for most of the tests.

This study was initiated to verify the effect of a pressure gradient on the boundary layer. This investigation involved situations in which the simple theory of reference 2 was inadequate since the pressure was poorly represented by the exponential law $p \propto x^n$ with a constant value for n, and the best approximate fit of the data for constant n produced values of n near the troublesome value of -1. Also, the local flow velocity was often less than hypersonic. The assumption of a local similarity concept, and thus a locally determined value of n, allowed the simple theory of reference 2 to be applied only on the leading 30 percent of the test area (ref. 3), and in this instance it did not agree with the trend of the data although there was agreement with the general level of the data.

The slightly more general exponential pressure law used in the method of the present author (ref. 3) extended its applicability to better cover the experimental cases involved in this investigation. To verify more completely the applicability of this method, the calculated heat-transfer results were compared with those computed by a well-established more complicated theory which involves a point-by-point machine solution of the boundary-layer equations of reference 6 with similarity assumed.

SYMBOLS

A	constant in assumed exponential pressure variation
a	velocity of sound
B	constant
$C_{D,le}$	drag coefficient of leading edge
C_F	total skin-friction coefficient on a flat plate, $\frac{1}{l}\int_0^l C_f\,dx$
C_f	local skin-friction coefficient
C_w	linear viscosity coefficient, $\frac{\mu_w t_\infty}{\mu_\infty t_w}$
C_μ	linear viscosity coefficient, $\frac{\mu' t_\infty}{\mu_\infty t'}$
c_p	specific heat at constant pressure
d	diameter of hemicylindrical leading edge
f	function of η related to stream function
G	function of wall temperature and specific heat ratio in laminar-boundary-layer growth equation
H	total enthalpy, $h + \frac{u^2}{2}$
h	local enthalpy, $c_p t$
I_1, I_2	integrals which represent solutions of boundary-layer equations

K_δ local inclination of boundary layer with respect to plate surface in hypersonic similarity form, $M_\infty \, d\delta/dx$

K_1, K_2, K_3, K_4, K_5 factors used to correct flat-plate boundary-layer calculations for pressure gradient effect

l total length of flate plate or total length of model

M Mach number

m pressure gradient parameter, $U_e = X^m$

N_{Pr} Prandtl number

N_{St} Stanton number

n constant in assumed exponential pressure variation

P ratio of local wall pressure to free-stream pressure, p_w/p_∞

p pressure

p_b pressure evaluated for blunt flat plate at 0^o angle of attack

p_v pressure caused by boundary-layer growth

p_w pressure evaluated for sharp flat plate at local inclination

R Reynolds number

S enthalpy function, $\frac{H}{H_e} - 1$

t temperature

U transformed velocity, $\frac{a_o}{a_e} u$

u air velocity relative to test surface

X transformed longitudinal coordinate, $\int_0^x \lambda \frac{p_e}{p_o} \frac{a_e}{a_o} dx$

x	longitudinal coordinate
Y	transformed normal coordinate, $\frac{a_e}{a_o}\int_0^y \frac{\rho}{\rho_o}\,dy$
y	normal coordinate
α	angle of attack
β	pressure gradient parameter, $\frac{2m}{m+1}$
γ	ratio of specific heats
δ	boundary-layer thickness
δ^*	boundary-layer displacement thickness
ϵ	function of γ, $1 - \frac{0.0048}{(\gamma - 1)^2}$
ζ	function defined in equation (A3)
η	similarity variable, $\frac{Y}{X}\sqrt{\frac{m+1}{2}\frac{U_e X}{\nu_o}}$
θ	boundary-layer momentum thickness
λ	linear viscosity coefficient, $\frac{\mu t_o}{\mu_o t}$
μ	dynamic viscosity
ν	kinematic viscosity
ρ	density of air
$\overline{\chi}_\infty$	viscous interaction parameter, $\frac{M_\infty{}^3\sqrt{C_\mu}}{\sqrt{R_{\infty,x}}}$

Subscripts:

e	evaluated at edge of boundary layer
i	evaluated at reference position

l	evaluated at trailing edge of flat plate
o	evaluated at free-stream stagnation conditions
tr	transformed quantities
w	evaluated at wall conditions
x	evaluated at x distance from leading edge
∞	evaluated at free-stream conditions

Primes denote differentiation with respect to η or parameters evaluated by the T-prime method.

THEORY

Similarity has been achieved on a hypersonic transformed plane in reference 1 by assuming $p \propto x^n$. The relation between β and n shown in this reference has been used in reference 2 to evolve a very simple method for determining heat transfer, skin friction, and boundary-layer thickness (which has been shown nearly equal to displacement thickness in hypersonic flow) in hypersonic flow with a pressure gradient. In this same reference, however, it is demonstrated that the solutions become imaginary, and thus invalid, as $n \to -1$.

The details of a theoretical method by the present author for calculating characteristics of the laminar boundary layer are shown in reference 3. This method involves the more general assumption of $p \propto (x + A)^n$ and does not require the assumption of hypersonic flow conditions. These assumptions, along with boundary-layer growth in a constant entropy field and the perfect gas equation of state, are applied to the $N_{Pr} = 1$ solutions of references 4 and 5 to produce solutions in closed form. Calculations by this method are shown in reference 3 which do not become imaginary for a pressure gradient described by a value of n less than -1, and for local flow conditions less than hypersonic. A summary of the theoretical results shown in reference 3 are given in appendix A.

Experimental pressures were used to determine the constants A and n utilized in the theory of reference 3. Theoretical estimates of these pressures by a simple hypersonic method were tried with varying degrees of success. Explanation of this method and the results are shown in appendix B.

Subsequent applications of relations given in reference 3 showed that, for small values of A and for values of n approaching -1, the calculated parameters were unrealistically sensitive to small changes in the value of A. This application is approaching the area for hypersonic flow where the relations of reference 3 reduce to those of reference 2, and where those of reference 2 are imaginary. A study of the parameters involved shows that when n is negative, the assumption $p \propto x^n$ produces an infinite pressure on the stagnation line. Even more unrealistic is the fact that when n approaches $\frac{-2\gamma}{3\gamma - 1}$ (-7/8 for air), the integral for the longitudinal coordinate transformation used in references 2 to 5 $\left(X = \int_0^x \lambda \frac{p_e a_e}{p_o a_o} dx\right)$ fails to converge. The modified assumption $p \propto (x + A)^n$ prevents the infinite pressure predicted at $x = 0$ for a negative n when A has a positive finite value and also prevents the divergence of the integral in the longitudinal coordinate transformation. The parameter arising from this integral which applies to the theory directly is $\frac{m + 1}{2} \frac{x}{X} \frac{dX}{dx}$. When $A = 0$ and $t_e/t_o = 0$, the value of this parameter may be expressed as follows:

$$\frac{m + 1}{2} \frac{x}{X} \frac{dX}{dx} = \frac{n + 1}{2}$$

It is apparent that this relation shows no discontinuities or irregularities in the neighborhood of $n = -7/8$. Thus, another consideration must be examined to learn the consequences of the nonconvergence of this integral when $A = 0$ and $t_e/t_o = 0$.

If the pressure is assumed to vary as $p \propto (x + A)^n$, then $\frac{dP}{dx} = \frac{nP}{x + A}$ or $\frac{x}{P} \frac{dP}{dx} = \frac{n}{1 + \frac{A}{x}}$. If a constant pressure and pressure gradient are considered for a station x_i, $\frac{x}{P} \frac{dP}{dx}$ is constant and n is a function of A at this station x_i. The effect of a change in the values of A/x_i and n on the shape of the pressure curve when n is negative is illustrated in figure 1(a). It is clear that families of curves mutually tangent at a point all have the same value of $\frac{x}{P} \frac{dP}{dx}$ at that point, and that curves of each family with increasing curvature have increasing values of A/x_i and increasing negative values of n. The effect that $\frac{x}{P} \frac{dP}{dx}$, A/x_i, and n have upon the heat transfer is given in figure 1(b) where the heat-transfer parameter has been calculated for the hypersonic case ($t_e/t_o = 0$), for $\gamma = 1.4$, and for $N_{Pr} = 0.7$. The heat transfer is reduced for increasingly negative values of $\frac{x}{P} \frac{dP}{dx}$. Also, at all values of $\frac{x}{P} \frac{dP}{dx}$, the effect of A/x_i upon the heat transfer is reduced at large values of A/x_i. At values of $\frac{x}{P} \frac{dP}{dx}$ near zero, the effect of A/x_i upon the heat transfer is small at all values of A/x_i, but at values of $\frac{x}{P} \frac{dP}{dx}$ approaching $\frac{-2\gamma}{3\gamma - 1}$ (-7/8 for air), the values of calculated heat-transfer parameters are very sensitive to small changes in A/x_i when A/x_i is near zero. The rapid change in these calculated values is apparently beyond that which should be expected from

physical considerations. This effect is the apparent consequence of the previously mentioned singular integral. This characteristic of the theory will be recalled subsequently during the comparison of theory and data.

EXPERIMENTAL APPARATUS

Tunnel and Test Conditions

The experimental temperature pressure and visual flow measurements were made in the Langley 11-inch hypersonic tunnel in the $M = 7$ and $M = 10$ air nozzles. The Mach 7 nozzle is a two-dimensional nozzle constructed of Invar since this metal has a very low temperature coefficient of expansion. Thus, the temperature strain of the first minimum during a test was low and the variation of Mach number with time was less than that expected for an identical steel nozzle. The unit Reynolds number for these tests was from 5×10^6 per meter to 14×10^6 per meter. The Mach 10 nozzle is a three-dimensional nozzle so that the temperature strain near the first minimum has little effect on its effective area, and the Mach number does not vary during a run with constant stagnation conditions. The unit Reynolds number per meter for the tests in this nozzle varied from 2.5×10^6 to 5×10^6. The air supplied these nozzles is dried by being pumped through a silica gel drier as it is stored at 50 atmospheres pressure before it enters the storage tank. During a test the air enters the nozzle after passing through an adjustable pressure-regulating valve, an electrical heater with nickel-chromium-alloy heating elements, and a settling chamber where the vorticity and contamination of the air are reduced by screening. An adjustable second minimum and a diffuser followed by a water-cooled heat exchanger downstream of the test region delays the pressure rise in the vacuum tank and thus delays the breakdown of the flow in the test nozzle. Many of the details of construction, calibration, and instrumentation of this intermittent facility are reported in references 7 to 10.

The Reynolds numbers of the tests in the $M = 7$ nozzle were approximately 1.0×10^6, 1.5×10^6, 2.0×10^6, and 2.8×10^6 based on free-stream conditions and the total length of the curved plate. The Mach number for these tests varied slightly with tunnel position, stagnation pressure, and elapsed time from the start of the test but always fell in the range 6.6 to 6.9. The Mach number variation with time and with stagnation pressure was accounted for in the calculation of the pressure and heat-transfer parameters. The stagnation temperatures fell in the range between 585° K and 655° K but varied much less than this during a single test.

The Reynolds numbers of the tests in the $M = 10$ nozzle were approximately 0.5×10^6 and 1.0×10^6 based on free-stream conditions and the total length of the model.

The Mach number was between 9.5 and 9.75 and varied with tunnel position and stagnation pressure. The stagnation temperature for these tests varied from 820° K to 880° K.

Models and Instrumentation

The model profile used in this research program was a cylindrical leading edge followed by identical curved surfaces with one convex face and one concave face exposed to the airstream. The curvature of these surfaces was determined as shown in figure 2 from the relation $y/B = (x/B)^{5/8}$, started with a slope of $\pi/3$ ($x/B = 0.0662$), and continued until x/B reached a value of 5/8 and the surface inclination was $\pi/5$. This arc was the generator of the airfoil's lower surface and was rotated $\pi/18$ and translated a sufficient distance to join the nose profile to become the airfoil's upper surface. The nose profile was a cylinder of 6.35-mm diameter followed by wedge surfaces, 1.6 mm long with $\pi/18$ included angle, tangent with the two airfoil surfaces. The position of this wing resting on a flat surface was defined as the zero angle of attack of the wing, the base was normal to this flat surface, and the upper surface was extended to meet it.

In this investigation two models were tested at angles of attack of -8°, 0°, and 15°. The positive angle was defined with the concave surface exposed to the flow. The three angles which were chosen were such that the concave surface near the trailing edge was alined with the stream at $\alpha = -8°$, the convex surface near the trailing edge was alined with the stream at $\alpha = 0°$, and the convex surface near the leading edge was alined with the stream at $\alpha = 15°$.

One of the test models was constructed of solid aluminum and contained no instrumentation. This model, shown in figure 3, was sting mounted and was used to study the shock formation and surface shear by means of schlieren and oil-flow studies.

The other model was constructed of 1.27-mm-thick Inconel sheet mounted on a steel frame as shown in figure 4. Temperature and pressure measuring stations were provided on both the concave and convex surfaces of this model, and removable end plates were supplied. The numerous pressure and temperature leads required the model to be side mounted. A photograph of the model in place is shown in figure 5.

The transient skin temperatures were measured by chromel-alumel 30-gage (0.254-mm-diam.) thermocouple wire spot-welded to the inner surface of the 1.27-mm-thick skin of the model. The two wires approaching each measuring station were shaped so that they diverged and then turned toward each other on an axis normal to the air flow. The two wires were spot-welded in this position not more than 1.6 mm apart. Thus, the output of each thermocouple station represented the average temperature over a lateral distance of as much as 1.6 mm but over a longitudinal distance of less than 0.25 mm (the diameter of the thermocouple wire). The thermoelectric signals from these stations were

indicated and recorded on fast-response 18-channel galvanometer oscillographs. The cold junctions were located in a junction box in close proximity with a thermometer and shielded from rapid changes in ambient temperature by insulation. Calibration of the galvanometers was accomplished by impressing measured currents through precision resistances in series with the measuring stations and the galvanometers.

Pressure orifices 1.52 mm in diameter were secured in place with silver solder at each pressure-measuring station. Leads no longer than 125 cm were connected with the six-cell aneroid-type recording instruments described in reference 7. The test chamber was evacuated prior to the test to prevent pressure errors from outgassing of the lines. The total temperature in the settling chamber was measured by bare wire thermocouples located at different radial stations and recorded on self-balancing 12-channel recorders. Stagnation pressures were observed on high-accuracy Bourdon tube type of pressure gages as well as on one cell of the fast-response instruments previously mentioned. The film record of the total pressure was examined to confirm instant establishment of the test pressure and to synchronize the timing of the test measurements.

Temperature Data Reduction

The heat transfer to this model was determined from the transient temperature response of the model skin near the start of the test. This method is explained in detail in reference 11. Sample conduction calculations indicate that conduction contributions were no more than 1 percent of the measured heating. Therefore, the experimental results are presented without conduction corrections. The recovery temperatures used to reduce local heating rates to local film coefficients of heat transfer were calculated from measured local pressures. Flow conditions at the outside edge were determined from an assumed isentropic expansion from the total pressure behind a normal shock. The recovery factors used were the square root of the local Prandtl numbers evaluated at temperatures calculated from Monaghan's T' method (ref. 12).

RESULTS AND DISCUSSION

The nature of the flow about this blunted curved plate may be learned from the schlieren pictures of the flow about the uninstrumented sting-mounted model with no end plates (fig. 6). The detached shock which wraps itself around the body is nearly symmetric about an axis not alined with the free stream. For the present tests, this shock envelope is more nearly alined with the free stream when $\alpha = 15^{\circ}$. At this angle of attack, the breadth of the shock envelope is a minimum.

There is little optical evidence that the boundary layer is separated either on the convex or on the concave surface of the wing. The schlieren photographs show a weak

shock formation initiated as a coalescence of compression waves emanating from the concave surface of the wing about three diameters behind the leading edge. The expansion waves at the base of the vehicle are those expected for an attached boundary layer.

Two schlieren photographs are presented for flow at $\alpha = 15^{\circ}$, $M = 6.8$, and $R_{\ell} = 7.3 \times 10^{6}$. Both photographs are data from the same test at different times. Although the shock about the model appears the same in both, tunnel wall separation is evident in one and not in the other. Such unsteady flow phenomena have previously been reported in situations with separated flow (refs. 11 and 13). When the model with the pressure and temperature instrumentation was in place, the tunnel blockage was greater than when the visual flow sting-mounted model was in place. Therefore, when the pressure data from some tests exhibited rapid fluctuations and failed to correlate well, the results from these tests were assumed to be faulty because of tunnel interference and were discarded.

End Plates

Oil-flow photographs in figure 7 show the direction and relative intensity of the surface shear. The flow on the plate caused by the tip effect is shown clearly in the oil-flow photographs. Along the center line where the instrumentation is concentrated, the end flow appears to be small, and the use of end plates might be considered unnecessary. Nevertheless, in an attempt to obtain better two-dimensional flow over the test surfaces, end plates were used while most of the data were obtained. Subsequent oil-flow photographs show that weak shocks caused by shock boundary-layer interaction in corner flow where the end plates attach to the wing also interfere with two-dimensional flow.

The heat transfer and pressure data may be examined to show the difference accorded by the presence or absence of end plates. Figure 8 was prepared to compare these results, which are shown only for $M = 6.8$. The data at $M = 9.6$ followed the same trend as the lower Mach number data with a little more scatter. On the convex surface, the pressure data with end plates fall above the data without end plates. At -8° angle of attack, the data are evidently increased about 20 percent near the trailing edge. At 0° angle of attack, the magnitude of the effect upon pressure was about the same. At 15° angle of attack, the pressure data gave evidence of separation on the convex surface. This evidence was seen both with and without the end plates. The separation appears somewhat more extensive with the end plates. The effect of the end plates on the heat transfer to the convex surface is partly obscured by scatter, but appears to be less than that on pressure. Most of the end-plate effect on the heat-transfer parameter at $\alpha = -8^{\circ}$ and at $\alpha = 0^{\circ}$ is in the opposite direction of the effect on the pressure. Thus, the parameter $N_{St,\infty}\sqrt{R_{x,\infty}}$ can be expected to correlate the data better for $\alpha = -8^{\circ}$ and 0°. For the 15° angle of attack, however, the parameter used correlated the heat-transfer

data very well even though the pressures vary by as much as a factor of 2. Both with and without end plates, however, the heat-transfer data for $\alpha = 15^{\circ}$ indicate a small region of laminar separation followed by transition. On the concave surface the effect of the end plates on the pressure and the heat-transfer data is not as clear as the effect on the data on the convex surface. At $\alpha = -8^{\circ}$ the end plates apparently cause the data with end plates to scatter near the trailing edge. This scatter is possibly caused by transitional flow along one row of thermocouples and laminar flow along another row. At $\alpha = 0^{\circ}$ the end plates have more effect on the pressure and less on the heat transfer, whereas at $\alpha = 15^{\circ}$ the effect of the end plates on both the pressure and heat transfer is small.

There is little question that weak shocks generated by end plates affected part of the experimental results by changing the pressure slightly and by affecting the location of the start of transition. Their absence, however, led to the signal seen in the oil-flow data fostered by the tip vorticity and transmitted obliquely along the surface. Thus, the benefit of using end plates is unresolved.

Convex Surface

The experimental pressures on the convex surface of the curved plate are shown in figure 9. End plates were used in this and all subsequent data in this report. The trend of these data is well represented by the empirical power law pressure distributions which were used to calculate the heat-transfer theory. The experimental and theoretical heat-transfer results for the corresponding cases are also shown in figure 9. Most pressure data for a given test Mach number and angle of attack appear little affected by the range of Reynolds numbers used in the tests, and most of the heat-transfer results are likewise little affected by the Reynolds number variation.

At -8° and 0° angles of attack, no part of the convex surface was at a negative inclination to the stream. The base pressure was below stream and there was thus no downstream pressure rise to be transmitted forward through the boundary layer. The pressure decreases monotonically from the leading edge to the trailing edge. The experimental heat-transfer results agree in general level and trend with the laminar theory. The boundary layer is thus established as laminar and attached.

At 15° angle of attack, the convex surface was inclined at negative angles approaching 15° at stations toward the trailing edge. The possibility of forward transmittal of a downstream pressure rise was thus presented by this configuration. The resulting evidence of separation at $M = 6.8$ is seen in figure 9(e). The deviation from the pressure trend expected for attached flow indicates possible separation over the last one-third of the wing's surface. Only a hint of the anticipated reduction in heat transfer usually associated with laminar separation is observed, however, and this apparently

occurs near the start of separation. The steep increase in heat transfer after separation indicates the possibility of transition on the less stable separated boundary layer.

The experimental pressure results for $\alpha = 15^{\circ}$ determined at $M = 9.6$ for the convex surface in figure 9(f) do not show separation with the same degree of certainty as was shown for $M = 6.8$. However, the reduced heating on the final one-third of the wing surface is an indication of the thickening of the boundary layer just prior to separation, if not the actual separation. The pressure never reaches free stream as it did at the lower Mach number due to the blast-wave effect of the leading edge. The higher pressure on the concave side of the wing caused the higher base pressure which was transmitted forward on the convex surface. The sharp increase in heat transfer seen just ahead of the trailing edge at the greater Reynolds number again signifies the possible start of transition on a separated boundary layer.

A detailed examination of the theoretical and experimental heat-transfer results for figures 9(a) to 9(e) shows good agreement between the theory of reference 3 and the elaborate machine calculation. The data fall from only slightly below the theory to approximately 30 percent below the theory. The same comparison between the theoretical values calculated by the two methods and between the theoretical values and the data was expected for $\alpha = 15^{\circ}$ on the convex surface at $M = 9.6$. The greater scatter in the pressure data for this experimental case increased the uncertainty in determining the power law pressure function for use in the heat-transfer theory. As seen in figure 9(f), a straight line appeared to fit the data within the tolerance suggested by the scatter. For this data fit, $A = 0$, and the negative value of n determined was only slightly less than 0.875, the value of $\frac{2\gamma}{3\gamma - 1}$ for air. The resulting theoretical values of the heat-transfer parameter determined by the two methods from this set of conditions failed to show the same agreement and to exhibit the correlation with the data expected from previous results. As a first attempt to understand the lack of agreement between the two theoretical methods, a different power law variation of pressure was determined with an arbitrary value of 1 for A, and with the curve constrained to pass through two points near the ends of the previous p versus x function. As may be observed from figure 9(f), this pressure curve is very slightly different from that with $A = 0$ and agrees with the pressure data as well as the first trial. The negative value of n specified is slightly greater than 0.875 rather than slightly less. The theoretical heat-transfer results determined by the theory of the present author for this slight perturbation in faired pressures was increased by approximately 50 percent and moved from a position below the data to one above the data. The values determined by the method of reference 6 were only slightly affected by this trivial change in the pressure distribution and were thus bracketed by the two theoretical results realized from the simple theory.

The extreme sensitivity of the values calculated by the method of the present author (ref. 3) to small changes in the value of A when A is small is discussed in the section entitled "Theory." Notice that the limiting values of p/p_∞ as x approaches 0 for these two assumed power law pressure functions are ∞ and 39, whereas the correct stagnation line value is 119. When a third power law pressure function was devised which was constrained to pass through the same end points and to predict the correct pressure on the stagnation line, it followed a path between those of the first two pressure functions. The heat-transfer values calculated with this third power law pressure function are in good agreement with the results of the complete machine solution of the boundary-layer equations of reference 6, and the theories agree well with the data. This agreement may be taken as an indication that, as A tends toward zero and n tends toward $-2\gamma/(3\gamma-1)$, the closed-form solution of reference 3 will give reliable results if the assumed power law pressure function is constrained to predict the correct pressure on the stagnation line.

Concave Surface

The pressure distribution and heat transfer on the concave surface of the blunted curved plate is seen in figure 10. The effect of the changing Reynolds number has little effect on the pressure distribution for any of the three angles of attack at $M = 6.8$; this suggests attached flow on the lower surface. The blast-wave effect combines with the power law curvature of the lower surface to cause relatively constant pressure over the forward two-thirds of the surface at -8° angle of attack, over the forward one-half of the surface at 0° angle of attack, and over the forward one-third of the surface at 15° angle of attack. To the rear of these constant-pressure areas, the pressure trend is toward increasingly severe adverse pressure gradients at higher angles of attack.

The heat-transfer results at $M = 6.8$ are little affected by the varying Reynolds number on the part of the concave surface where the pressure is constant, but they are greatly affected by the changing Reynolds number in the region of adverse pressure gradient. For -8° and 0° angles of attack, the heat-transfer data at the lowest Reynolds number suggest laminar flow, and the data at increasing Reynolds numbers suggest transitional flow. At 15° angle of attack, none of the data suggested laminar flow over the entire surface. Increasing Reynolds numbers were accompanied by an apparent forward movement of the start of transition.

The theoretical heat transfer to the concave surface in the region of constant pressure is another example of variance between results obtained from the two theoretical methods. The disagreement is most apparent for -8° angle of attack. It is also obvious that the theory of reference 6 involving the machine calculation is in better agreement with both the level and the trend of the heat-transfer data. Remember that the integral

associated with the transformed streamwise coordinate in the theory of reference 6 is evaluated from the stagnation point of the blunt leading edge by the use of the Newtonian pressure distribution around the cylinder, whereas the closed-form solution by the present author (ref. 3) does not account for this leading-edge bluntness in the analogous integral. In this instance the failure of the assumed power law pressure distribution to correctly predict pressures in the leading-edge region causes inaccuracy in this theoretical heat-transfer calculation. At the higher angles of attack of 0° and 15°, the two theoretical heat-transfer calculations are observed to approach each other at increasing angles of attack. This is expected since the integral of a higher nearly constant surface pressure function is less affected by the relatively smaller pressure perturbation near the leading edge.

CONCLUDING REMARKS

Pressure and heat transfer have been measured on convex and concave curved surfaces following a hemicylindrically blunted leading edge at Mach numbers of 6.8 and 9.6 and Reynolds numbers based on length from 0.5×10^6 to 3.0×10^6. The curvature of both surfaces was specified by the same power law relationship.

Power law functions were determined which fit the pressure data. The empirical constants were then used to calculate the heat transfer by a previously published closed-form solution by the present author (AIAA Journal, April 1967). This method used Prandtl number 1 $\left(N_{Pr} = 1\right)$ solutions of the laminar boundary layer with an arbitrary pressure gradient. These solutions were reduced to a closed form by assuming that the pressure varies as the power of the sum of the streamwise coordinate and an arbitrary constant or $p \propto (x + A)^n$. This condition permitted the evaluation of the streamwise coordinate transformation. Then the $N_{Pr} = 1$ solutions are expressible in a simple closed form in terms of physical quantities in the real plane. These theoretical values were compared with a point-by-point solution of the laminar boundary-layer equations by an iterative electronic computer method with similarity assumed and with the experimentally determined heat transfer. In most cases the two theories and the data were in good agreement. In some cases the simple theory of the present author gave less than desirable accuracy and certainty. The failure of the simple theory in these instances was attributed to the failure of the assumed power law to predict the correct pressure in the region of the leading edge. An example was shown where the assumed power law which adequately agreed with pressure aft of the leading edge was perturbed slightly with

a constraint to predict the stagnation line pressure accurately, and where the accuracy of the calculated results was improved.

Langley Research Center,
National Aeronautics and Space Administration,
Langley Station, Hampton, Va., June 13, 1967,
129-01-07-07-23.

APPENDIX A

A SUMMARY OF THE THEORETICAL RESULTS OF REFERENCE 3

The details of a simple theoretical method for calculating characteristics of the laminar boundary layer are shown in reference 3. This method involves the assumption of $p \propto (x + A)^n$, boundary-layer growth in a constant entropy field, and a perfect gas equation of state. These assumptions are applied to the $N_{Pr} = 1$ compressible solutions of the laminar boundary layer, that are shown in reference 4.

The boundary-layer thickness and the skin friction are little affected by the $N_{Pr} = 1$ assumption since the solution of the energy equations has little effect on these parameters. The heat-transfer calculations are directly involved with the solution of the energy equation and are corrected for $N_{Pr} = 1$ by the method suggested in reference 5. The final relations which involve no hypersonic assumptions appear as follows:

The relationship between the Falkner-Skan and the Li-Nagamatsu pressure gradient parameters is

$$m = \frac{n(1 - \gamma)}{(3\gamma - 1)n + 2\gamma}\left(\frac{1 - \zeta}{1 - \frac{t_e}{t_o}}\right) = \frac{n(1 - \gamma)}{2\gamma}\left(\frac{x}{x + A}\right)\left[\left(1 - \frac{t_e}{t_o}\right)\frac{x}{X}\frac{dX}{dx}\right]^{-1} \tag{A1}$$

$$\beta = \frac{2m}{m + 1} = \frac{n(1 - \gamma)(1 - \zeta)}{(n + 1)\gamma - \left[\frac{(3\gamma - 1)n + 2\gamma}{2}\right]\frac{t_e}{t_o} - \frac{\zeta n}{2}(1 - \gamma)} \tag{A2}$$

where

$$\zeta = \left(\frac{A}{x + A}\right)^{\frac{(3\gamma-1)n+2\gamma}{2\gamma}} \tag{A3}$$

The displacement and momentum thicknesses are

$$\frac{\delta^*}{x}\sqrt{R_{x,\infty}} = \left(\frac{p_\infty}{p_w} C_w\right)^{1/2} \frac{t_o}{t_\infty}\left[\frac{n(1 - \gamma)}{2\gamma\beta}\left(\frac{x}{x + A}\right)\left(\frac{1}{1 - \frac{t_\infty}{t_o}}\right)\right]^{-1/2}\left(\frac{1 - \frac{t_e}{t_o}}{1 - \frac{t_\infty}{t_o}}\right)^{1/4}\left[I_1 + \left(1 - \frac{t_e}{t_o}\right)I_2\right] \tag{A4}$$

$$\frac{\theta}{x}\sqrt{R_{x,\infty}} = \left(\frac{p_\infty}{p_w} C_w\right)^{1/2} \frac{t_o}{t_\infty}\left[\frac{n(1-\gamma)}{2\gamma\beta}\left(\frac{x}{x+A}\right)\left(\frac{1}{1-\frac{t_\infty}{t_o}}\right)\right]^{-1/2}\left(\frac{1-\frac{t_e}{t_o}}{1-\frac{t_\infty}{t_o}}\right)^{1/4}\left(\frac{t_e}{t_o} I_2\right) \tag{A5}$$

where

$$I_1 = \frac{\delta^*_{tr}}{X}\left(\frac{m+1}{2}\frac{U_e X}{\nu_o}\right)^{1/2} = \int_0^\delta (1 - f' + S)d\eta \tag{A6}$$

$$I_2 = \frac{\theta_{tr}}{X}\left(\frac{m+1}{2}\frac{U_e X}{\nu_o}\right)^{1/2} = \int_0^\delta f'(1 - f')d\eta \tag{A7}$$

The local and total skin-friction coefficients presented in a more accurate form than that seen in reference 3 are

$$C_{f,\infty}\sqrt{R_{x,\infty}} = \left(\frac{p_w}{p_\infty} C_w\right)^{1/2} 2f''_w\left[\frac{n(1-\gamma)}{2\gamma\beta}\left(\frac{x}{x+A}\right)\left(\frac{1}{1-\frac{t_\infty}{t_o}}\right)\right]^{1/2}\left(\frac{1-\frac{t_e}{t_o}}{1-\frac{t_\infty}{t_o}}\right)^{1/4} \tag{A8}$$

$$C_{F,\infty}\sqrt{R_{l,\infty}} = \left(\frac{p_w}{p_\infty} C_w\right)^{1/2} 2f''_w\left\{\left(\frac{2}{n+1}\right)\left[\frac{n(1-\gamma)}{\beta(n+1)\gamma}\right]\left(\frac{l+A}{l}\right)\left(\frac{1}{1-\frac{t_\infty}{t_o}}\right)\right\}^{1/2}\left(\frac{1-\frac{t_e}{t_o}}{1-\frac{t_\infty}{t_o}}\right)^{1/4}\left[1-\left(\frac{A}{l+A}\right)^{\frac{n+1}{2}}\right] \tag{A9}$$

The heat-transfer coefficient is shown as follows:

$$N_{St,\infty}\left(R_{x,\infty}\right)^{1/2} = \left(\frac{p_w}{p_\infty} C_w\right)^{1/2}\left(-\frac{S'_w}{S_w}\right)\left[\frac{n(1-\gamma)}{2\gamma\beta}\left(\frac{x}{x+A}\right)\left(\frac{1}{1-\frac{t_\infty}{t_o}}\right)\right]^{1/2}\left(\frac{1-\frac{t_\infty}{t_o}}{1-\frac{t_e}{t_o}}\right)^{1/4} N_{Pr}^{-0.6} \tag{A10}$$

The values of K_1 to K_5 may be evaluated in the frame of reference 2 without hypersonic approximations (with K_1, K_2, and K_4 appearing in more accurate form) and appear as follows:

APPENDIX A

$$K_1 = f''_w \frac{[2(1+n)]^{1/2}}{0.664}\left[\frac{1}{\beta}\left(\frac{n}{n+1}\right)\left(\frac{1-\gamma}{\gamma}\right)\left(\frac{x}{x+A}\right)\left(\frac{1}{1-\frac{t_\infty}{t_o}}\right)\right]^{1/2}\left(\frac{1-\frac{t_e}{t_o}}{1-\frac{t_\infty}{t_o}}\right)^{1/4} \tag{A11}$$

$$K_2 = \frac{f''_w}{0.332\,[2(1+n)]^{1/2}}\left[\frac{1}{\beta}\left(\frac{n}{n+1}\right)\left(\frac{1-\gamma}{\gamma}\right)\left(\frac{l+A}{l}\right)\left(\frac{1}{1-\frac{t_\infty}{t_o}}\right)\right]^{1/2}\left[1-\left(\frac{A}{l+A}\right)^{\frac{n+1}{2}}\right]\left(\frac{1-\frac{t_e}{t_o}}{1-\frac{t_\infty}{t_o}}\right)^{1/4} \tag{A12}$$

$$K_3 = \left(-\frac{S'_w}{S_w}\right)\frac{[2(1+n)]^{1/2}}{0.664}\left[\frac{1}{\beta}\left(\frac{n}{n+1}\right)\left(\frac{1-\gamma}{\gamma}\right)\left(\frac{x}{x+A}\right)\left(\frac{1}{1-\frac{t_\infty}{t_o}}\right)\right]^{1/2}\left(\frac{1-\frac{t_\infty}{t_o}}{1-\frac{t_e}{t_o}}\right)^{1/4} \tag{A13}$$

$$K_4 = \frac{2\left(\frac{1-\frac{t_e}{t_o}}{1-\frac{t_\infty}{t_o}}\right)^{1/4}}{[2(1+n)]^{1/2}\left[\frac{1}{\beta}\left(\frac{n}{1+n}\right)\left(\frac{1-\gamma}{\gamma}\right)\left(\frac{x}{x+A}\right)\left(\frac{1}{1-\frac{t_\infty}{t_o}}\right)\right]^{1/2}\left[I_1+\left(1-\frac{t_e}{t_o}\right)I_2\right]}}{(2)^{1/2}\left[I_1+\left(1-\frac{t_\infty}{t_o}\right)I_2\right]_{\beta=0}} \tag{A14}$$

$$K_5 = \frac{2\left(\frac{1-\frac{t_e}{t_o}}{1-\frac{t_\infty}{t_o}}\right)^{1/4}}{[2(1+n)]^{1/2}\left[\frac{1}{\beta}\left(\frac{n}{1+n}\right)\left(\frac{1-\gamma}{\gamma}\right)\left(\frac{x}{x+A}\right)\left(\frac{1}{1-\frac{t_\infty}{t_o}}\right)\right]^{1/2}\left(\frac{t_e}{t_o}I_2\right)}}{(2)^{1/2}\left(\frac{t_\infty}{t_o}I_2\right)_{\beta=0}} \tag{A15}$$

APPENDIX A

The relations for θ and K_5 were not defined or discussed in reference 2 or 3 and are therefore discussed as follows.

In a manner analogous to that given for the displacement thickness in reference 3, the expression for the momentum thickness is as follows:

$$\theta = \int_0^{\delta} \frac{\rho u}{\rho_e u_e}\left(1 - \frac{u}{u_e}\right)dy \tag{A16}$$

If constant pressure is assumed across the boundary layer, the expression for the momentum thickness in a perfect gas for $N_{Pr} = 1$ becomes

$$\theta = \frac{p_o a_o}{p_e a_e}\left(\frac{2}{m+1}\frac{\nu_o X}{Ue}\right)^{1/2}\left(\frac{t_e}{t_o}\right)\int_0^{\delta} f'(1 - f')d\eta \tag{A17}$$

Use of definitions from reference 2 allows equation (A17) to be simplified as follows:

$$\theta = \frac{p_o}{p_e}\left(\frac{t_e}{t_o}\right)^{1/2}\theta_{tr} \tag{A18}$$

or

$$\frac{\theta}{x}\left(R_{x,\infty}\right)^{1/2} = \left(\frac{p_\infty u_\infty}{p_w u_e} C_w\right)^{1/2}\left(\frac{t_o}{t_\infty}\right)\left(\frac{t_e}{t_o} I_2\right)\left(\frac{m+1}{2}\frac{x}{X}\frac{dX}{dx}\right)^{-1/2} \tag{A19}$$

If the assumption $p \propto (x + A)^n$ is made and the procedure shown in reference 3 is followed, the momentum thickness may be expressed in terms of real quantities

$$\frac{\theta}{x}\left(R_{x,\infty}\right)^{1/2} = \left(\frac{p_\infty}{p_w} C_w\right)^{1/2}\frac{t_o}{t_\infty}\left[\frac{n(1-\gamma)}{2\gamma\beta}\left(\frac{x}{x+A}\right)\left(\frac{1}{1 - \frac{t_\infty}{t_o}}\right)\right]^{-1/2}\left(\frac{1 - \frac{t_e}{t_o}}{1 - \frac{t_\infty}{t_o}}\right)^{1/4}\left(\frac{t_e}{t_o} I_2\right) \tag{A20}$$

When this equation is cast into the frame of reference 2,

$$\frac{\theta}{\bar{\theta}} = K_5\left(\frac{p_w}{p_\infty}\right)^{-1/2} \tag{A21}$$

where $\overline{\theta}$ represents the zero pressure gradient value with local conditions the same as the free stream. Then

$$K_5 = \frac{2\left(\frac{1 - \frac{t_e}{t_o}}{1 - \frac{t_\infty}{t_o}}\right)^{1/4}}{\left[2(1+n)\right]^{1/2}\left[\frac{1}{\beta}\left(\frac{n}{1+n}\right)\left(\frac{1-\gamma}{\gamma}\right)\left(\frac{x}{x+A}\right)\left(\frac{1}{1 - \frac{t_\infty}{t_o}}\right)\right]^{1/2}\left(\frac{t_e}{t_o} I_2\right)} \Bigg/ (2)^{1/2}\left(\frac{t_\infty}{t_o} I_2\right)_{\beta=0} \tag{A22}$$

APPENDIX B

THEORETICAL PRESSURES ON BLUNT CURVED PLATE

Numerous methods have been advanced for the determination of pressures on sharp or blunt plates in hypersonic flow. A method suggested in reference 14 has been tried for the calculation of the surface pressure in the present case. The method used was the linear combination of the local wedge pressure with the contributions expected for the blast-wave effect from the blunt leading edge and for the viscous effect from the growth of the displacement thickness as follows:

$$\frac{p}{p_\infty} = \frac{p_w}{p_\infty} + \frac{\Delta p_b}{p_\infty} + \frac{\Delta p_v}{p_\infty} \tag{B1}$$

The local wedge pressure was determined by the straightforward use of two-dimensional oblique shock or Prandtl-Meyer expansion theory for the pressure on a sharp flat plate at each local surface angle. The bluntness contribution was calculated by using equation (7) of reference 13 together with a correction suggested in reference 15

$$\frac{\Delta p_b}{p_\infty} = 0.187\epsilon\left(\sqrt{\gamma}(\gamma - 1)\frac{M_\infty^3 C_{D,le}}{x/d}\right)^{2/3} - 0.26 \tag{B2}$$

The viscous contribution was evaluated by the use of what was referred to as the "complete theory" in reference 15. This involved the use of equation (15) of reference 15 which is (in the terminology of this report)

$$\frac{\Delta p_v}{p_\infty} = \frac{\gamma(\gamma - 1)}{4}K_\delta^2 + \gamma K_\delta\sqrt{1 + \left(\frac{\gamma + 1}{4}K_\delta\right)^2} \tag{B3}$$

With equation (7) of reference 15, which is (in the terminology of this report)

$$K_\delta = \frac{K_4}{2}\frac{G\bar{\chi}_\infty}{\sqrt{p/p_\infty}}(1 - n) \tag{B4}$$

where K_4 was evaluated as suggested in reference 15. The calculations showed the viscous contributions to be negligible except at low pressure ratios.

The comparisons of these theoretical values with measured pressures are shown in figure 11. Comparisons on the convex surface are seen in figures 11(a) and 11(b) and agreement of level and trend is good. It is apparent, however, that agreement between

theory and data near the leading edge is better for $\alpha = 15^{o}$ than for the other two angles of attack. For $\alpha = 15^{o}$, the surface is at about zero inclination near the leading edge.

Comparisons of data and theory on the concave surface at $M = 6.8$ are shown in figure 11(c). In this figure, the linear combination of the two-dimensional expansion theory with the blast wave and viscous contribution has been less successful than for the convex surface. The poorest agreement is in the neighborhood of the nose for the wing at $\alpha = 0^{o}$ and $\alpha = -8^{o}$. For these angles of attack, a blunt leading edge is followed by a surface at a negative angle of attack not near zero. This failure of this method is pointed out in reference 14.

The pressure measurements on the concave surface at $M = 9.6$ showed the same trend as those at $M = 6.8$ but had greater scatter and are not included in figure 11.

REFERENCES

1. Li, Ting-Yi; and Nagamatsu, H. T.: Hypersonic Viscous Flow on a Noninsulated Flat Plate. GALCIT Mem. No. 25 (Contract No. DA-04-495-Ord-19), Apr. 1, 1955.

2. Bertram, Mitchel H.; and Feller, William V.: A Simple Method for Determining Heat Transfer, Skin Friction, and Boundary-Layer Thickness for Hypersonic Laminar Boundary-Layer Flows in a Pressure Gradient. NASA MEMO 5-24-59L, 1959.

3. Crawford, Davis H.: Applications of Similar Solutions for Calculation of Laminar Boundary-Layer Characteristics in the Presence of a Pressure Gradient. AIAA J. (Tech. Notes), vol. 5, no. 4, Apr. 1967, pp. 799-801.

4. Cohen, Clarence B.: and Reshotko, Eli: Similar Solutions for the Compressible Laminar Boundary Layer With Heat Transfer and Pressure Gradient. NACA Rept. 1293, 1956. (Supersedes NACA TN 3325.)

5. Cohen, Clarence B.; and Reshotko, Eli: The Compressible Laminar Boundary Layer With Heat Transfer and Arbitrary Pressure Gradient. NACA Rept. 1294, 1956. (Supersedes NACA TN 3326.)

6. Beckwith, Ivan E.; and Cohen, Nathaniel B.: Application of Similar Solutions to Calculation of Laminar Heat Transfer on Bodies With Yaw and Large Pressure Gradient in High-Speed Flow. NASA TN D-625, 1961.

7. McLellan, Charles H.; Williams, Thomas W.; and Bertram, Mitchel H.: Investigation of a Two-Step Nozzle in the Langley 11-Inch Hypersonic Tunnel. NACA TN 2171, 1950.

8. McLellan, Charles H.; Williams, Thomas W.; and Beckwith, Ivan E.: Investigation of the Flow Through a Single-Stage Two-Dimensional Nozzle in the Langley 11-Inch Hypersonic Tunnel. NACA TN 2223, 1950.

9. Bertram, Mitchel H.: Exploratory Investigation of Boundary-Layer Transition on a Hollow Cylinder at a Mach Number of 6.9. NACA Rept. 1313, 1957. (Supersedes NACA TN 3546.)

10. Bertram, Mitchel H.: Boundary-Layer Displacement Effects in Air at Mach Numbers of 6.8 and 9.6. NASA TR R-22, 1959. (Supersedes NACA TN 4133.)

11. Crawford, Davis H.: Investigation of the Flow Over a Spiked-Nose Hemisphere-Cylinder at a Mach Number of 6.8. NASA TN D-118, 1959.

12. Monaghan, R. J.: An Approximate Solution of the Compressible Laminar Boundary Layer on a Flat Plate. R. & M. No. 2760, Brit. A.R.C., 1953.

13. Crawford, Davis H.: The Effect of Air Bleed on the Heat Transfer and Pressure Distribution on 30° Conical Flares at a Mach Number of 6.8. NASA TM X-439, 1961.

14. Baradell, Donald L.; and Bertram, Mitchel H.: The Blunt Plate in Hypersonic Flow. NASA TN D-408, 1960.

15. Bertram, Mitchel H.; and Blackstock, Thomas A.: Some Simple Solutions to the Problem of Predicting Boundary-Layer Self-Induced Pressures. NASA TN D-798, 1961.

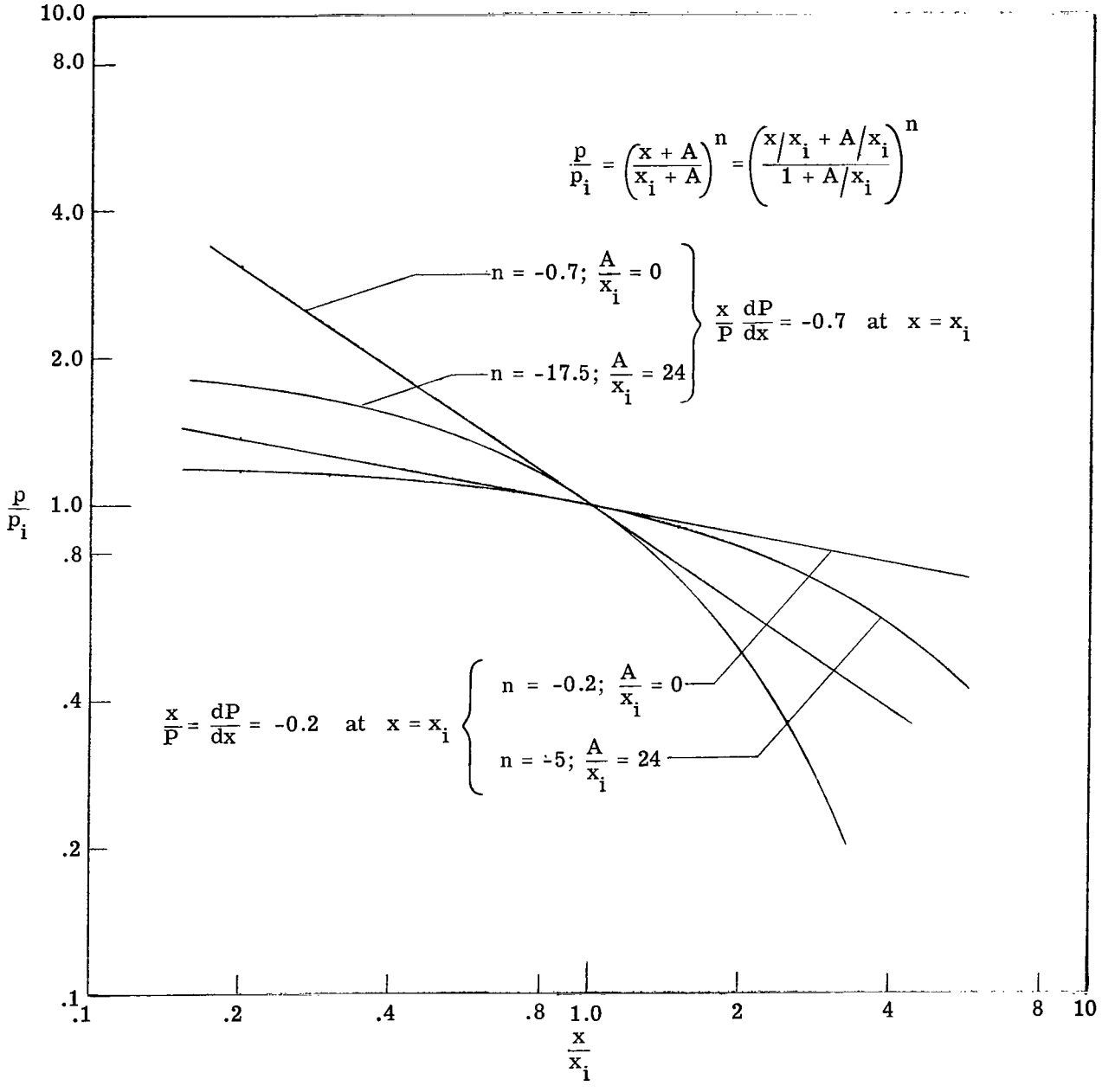

(a) Pressure distributions for assumed values of A/x_i and n.

Figure 1.- Effect of assumed values of A/x_i and n on calculated values of heat transfer in a favorable pressure gradient.

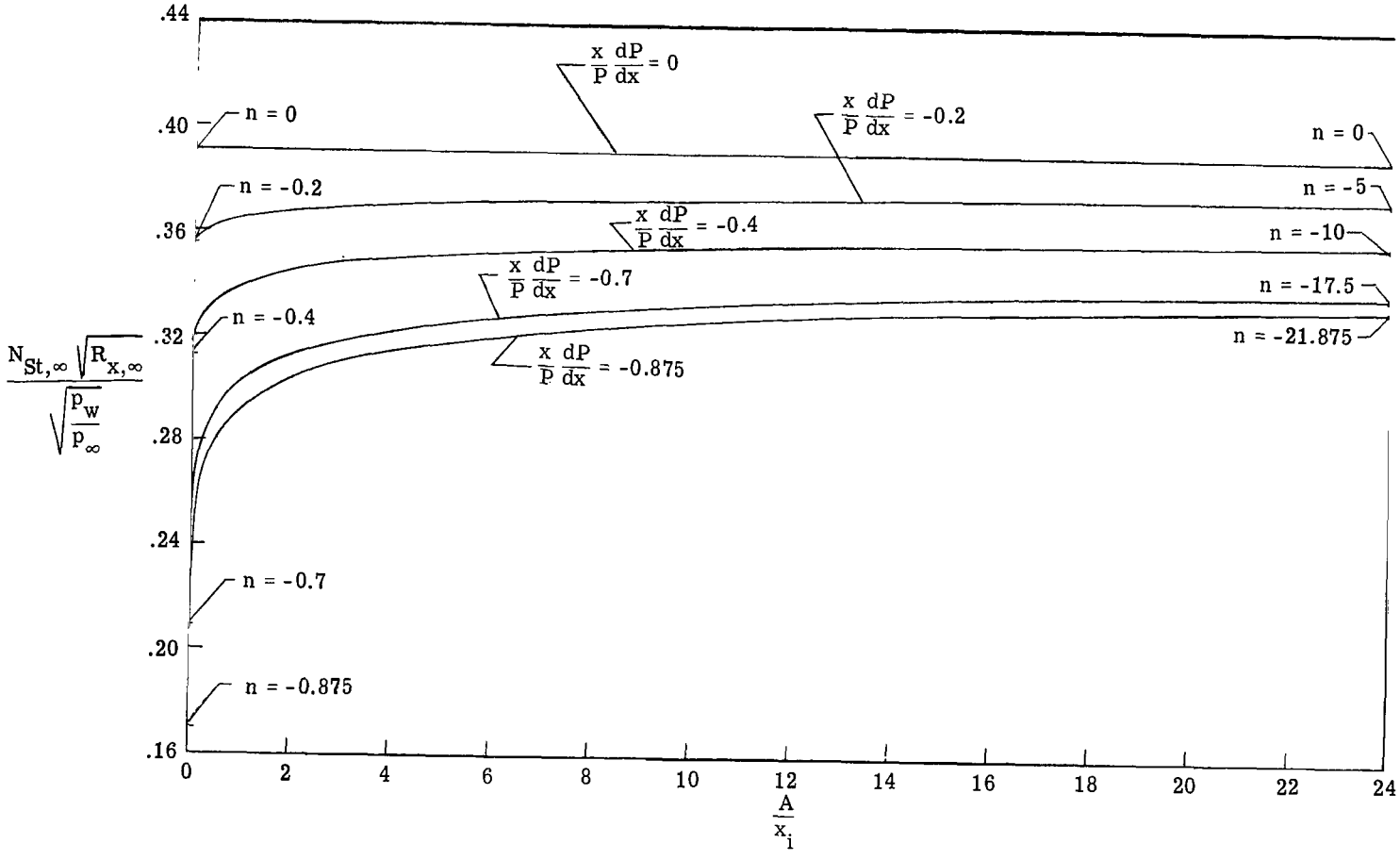

(b) Heat transfer.

Figure 1.- Concluded.

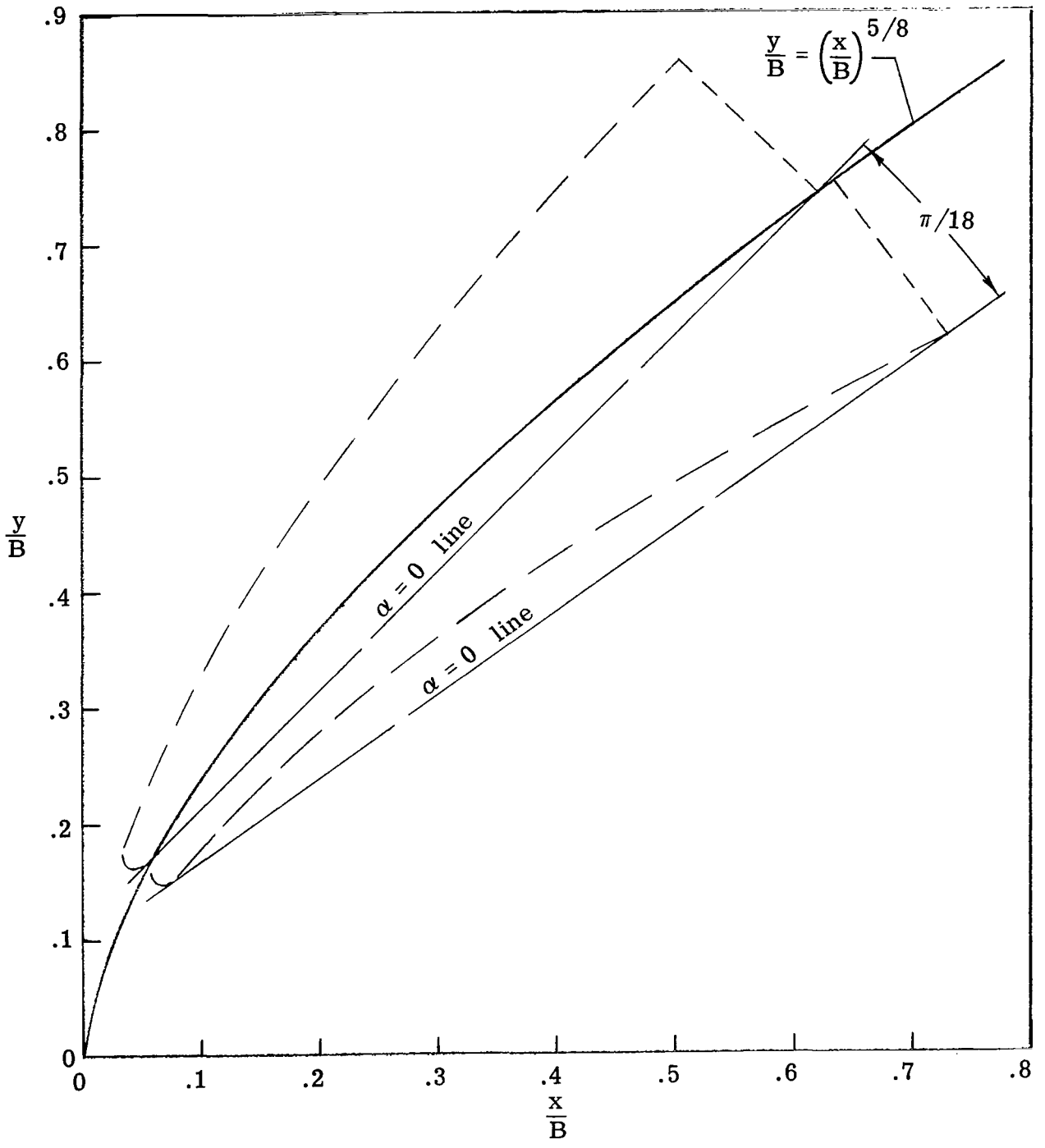

Figure 2.- Detail of curvature of model surface.

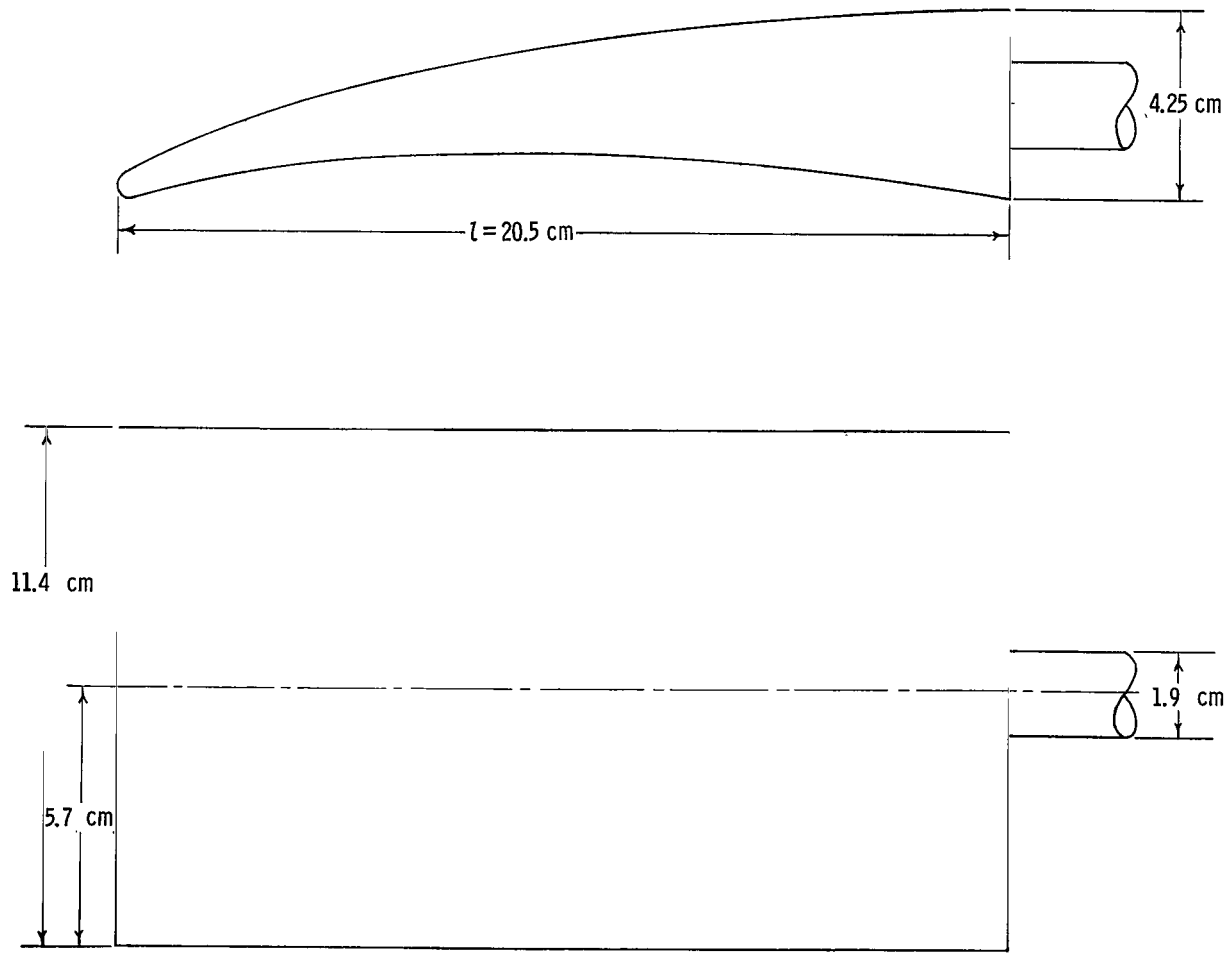

Figure 3.- Flow visualization model.

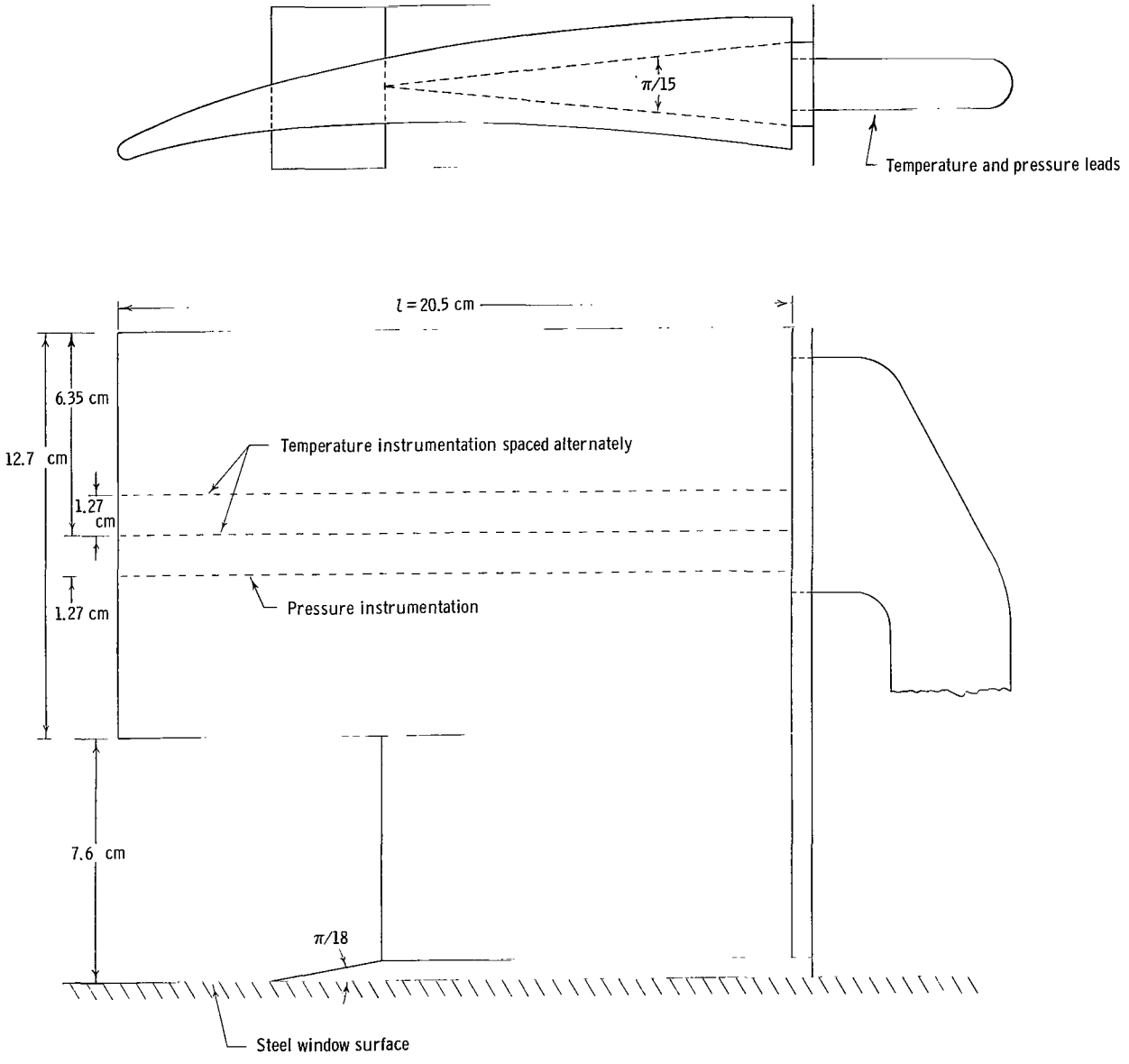

(a) Detail of concave surface.

Figure 4.- Heat transfer and pressure model.

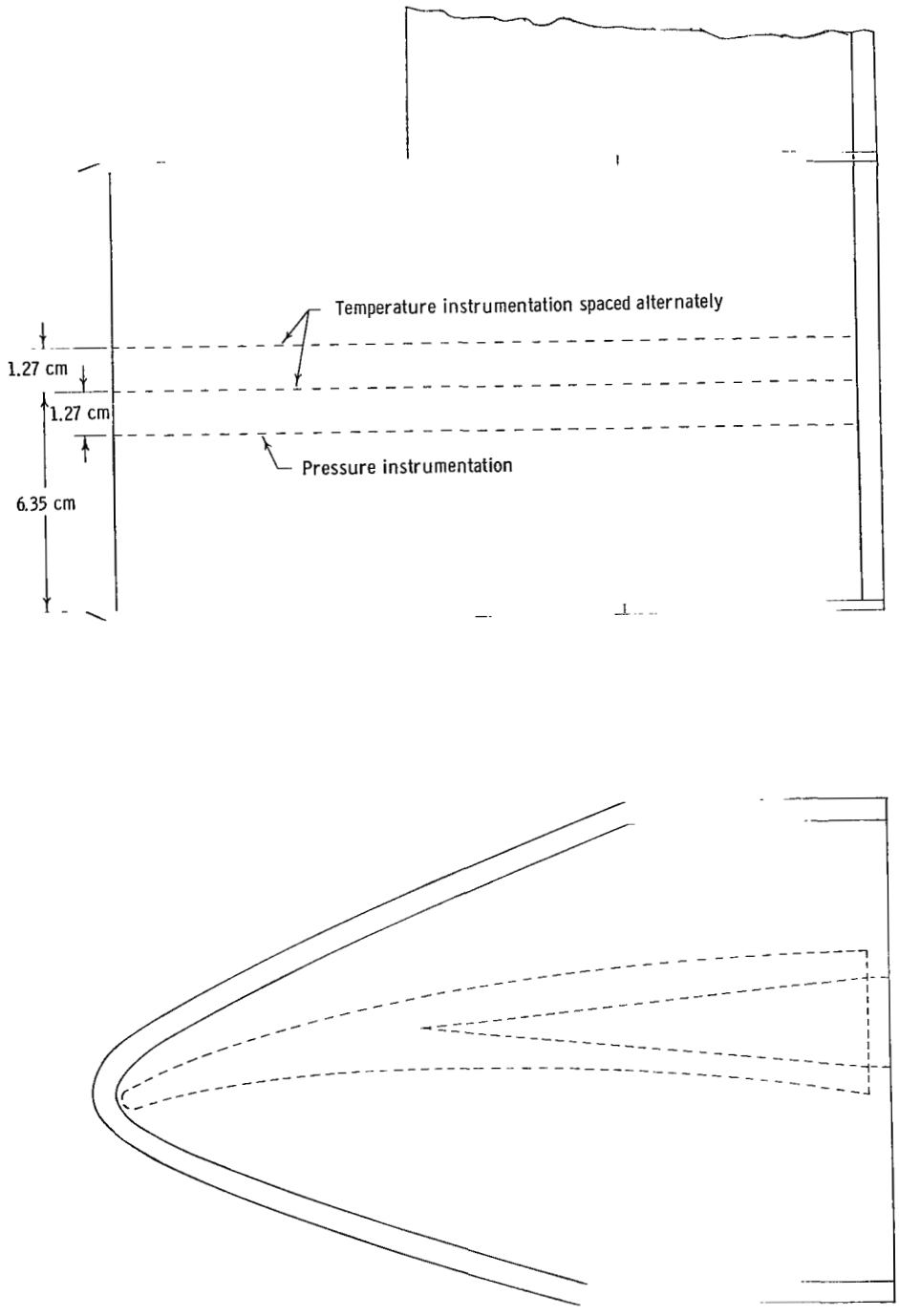

(b) Detail of convex surface and end plates.

Figure 4.- Concluded.

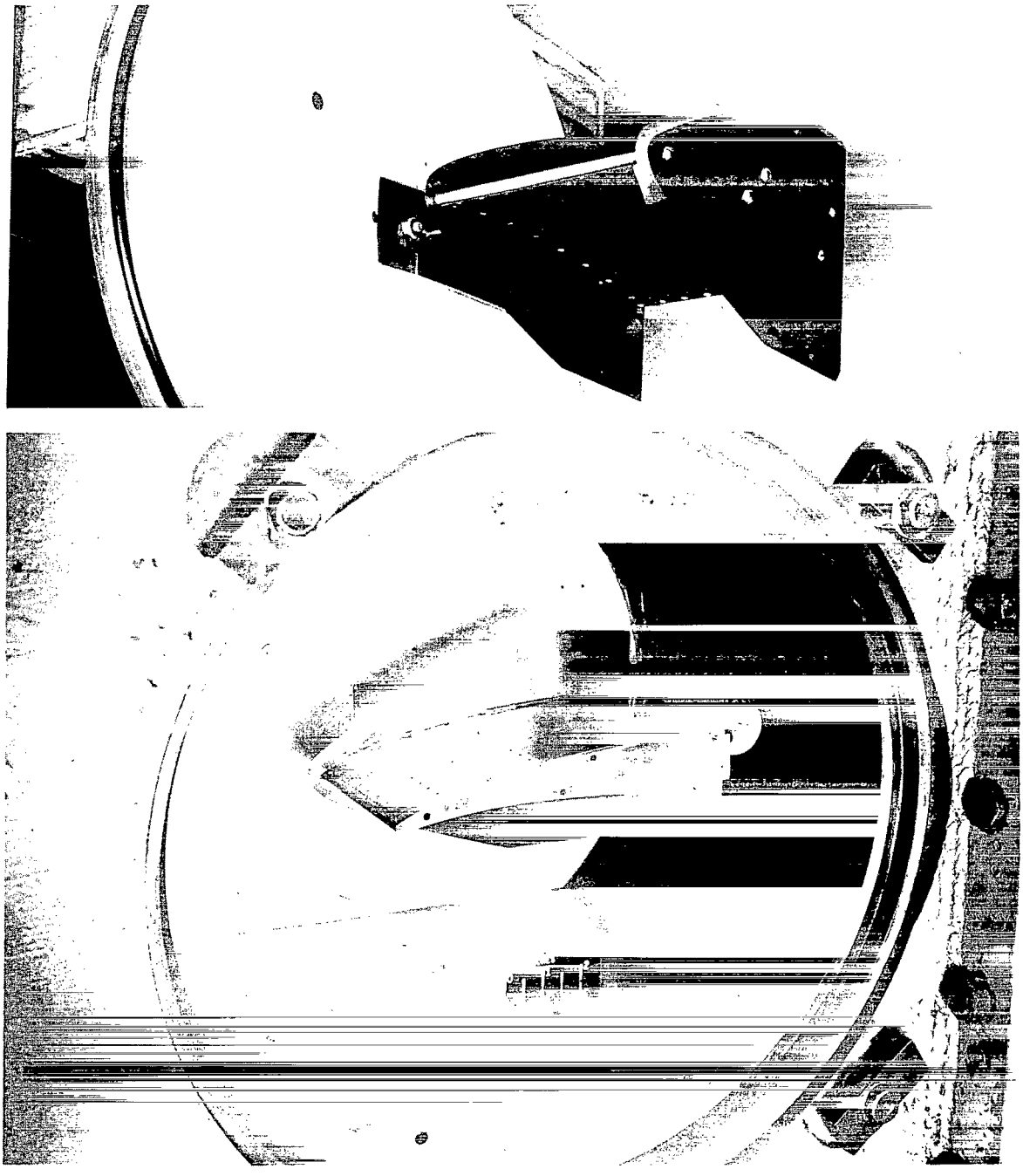

Figure 5.- Instrumented model. L-67-6606

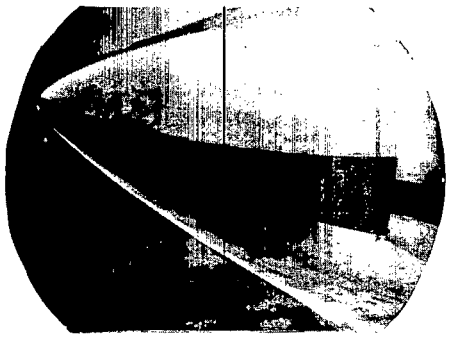

$\alpha = -8^{o}$

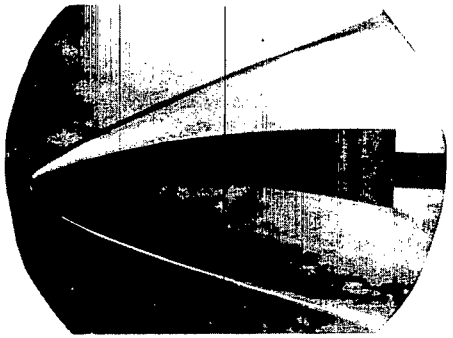

$\alpha = 0^{o}$

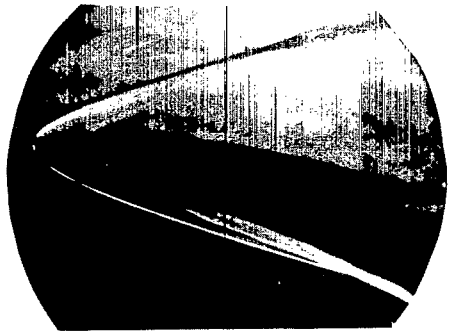

$\alpha = 15^{o}$

M = 9.6

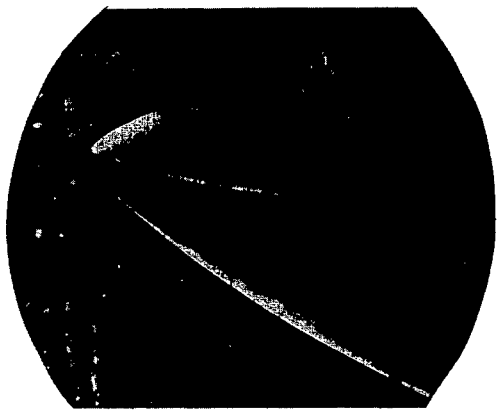

$\alpha = -8^{o}$

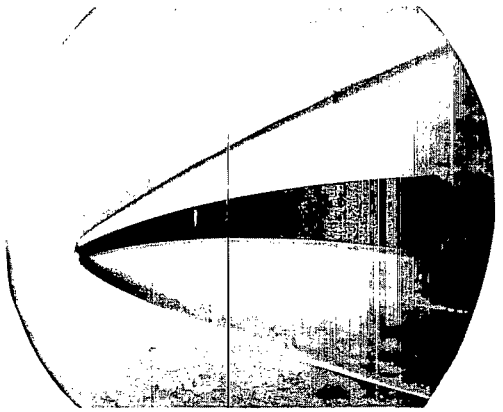

$\alpha = 0^{o}$

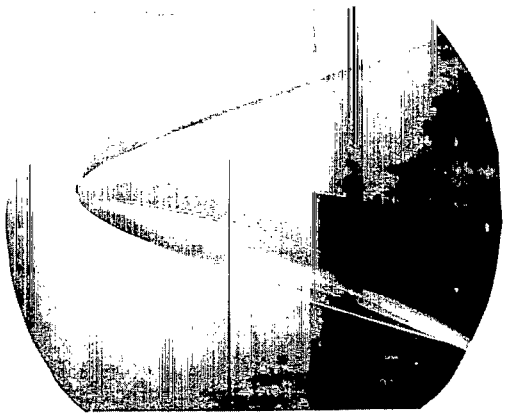

$\alpha = 15^{o}$

M = 6.8

(a) $R_{\ell} = 2.4 \times 10^{6}$. L-67-6607

Figure 6.- Schlieren photographs of flow about sting-mounted model with no end plates.

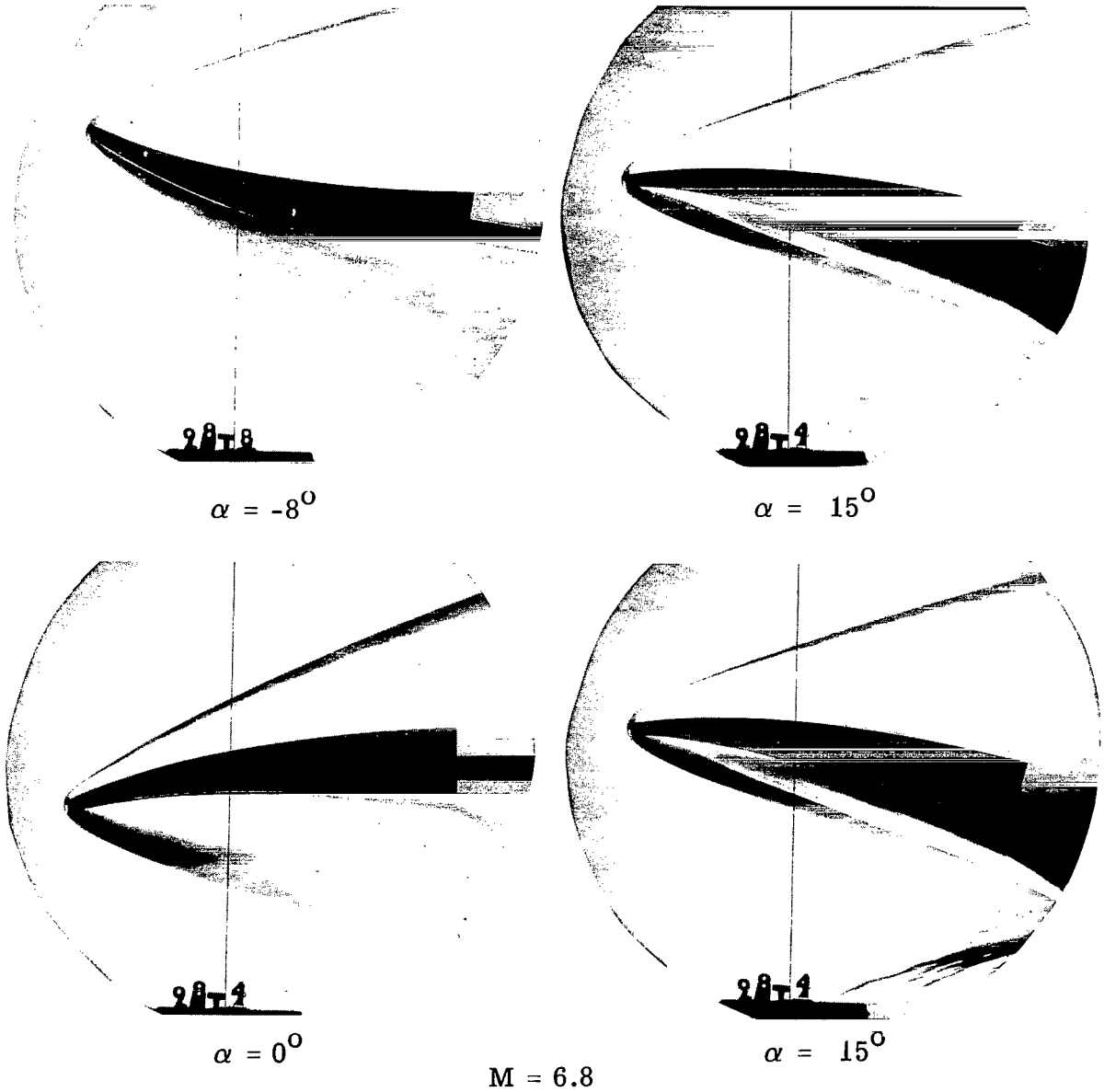

(b) $R_l = 7.3 \times 10^6$.

L-67-6608

Figure 6.- Concluded.

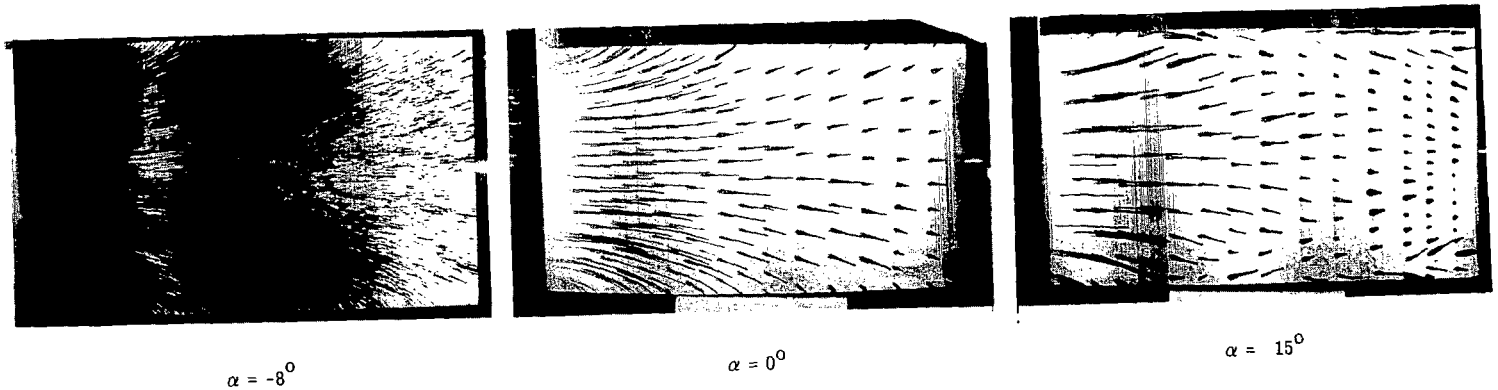

$\alpha = -8^{o}$ $\alpha = 0^{o}$ $\alpha = 15^{o}$

No end plates

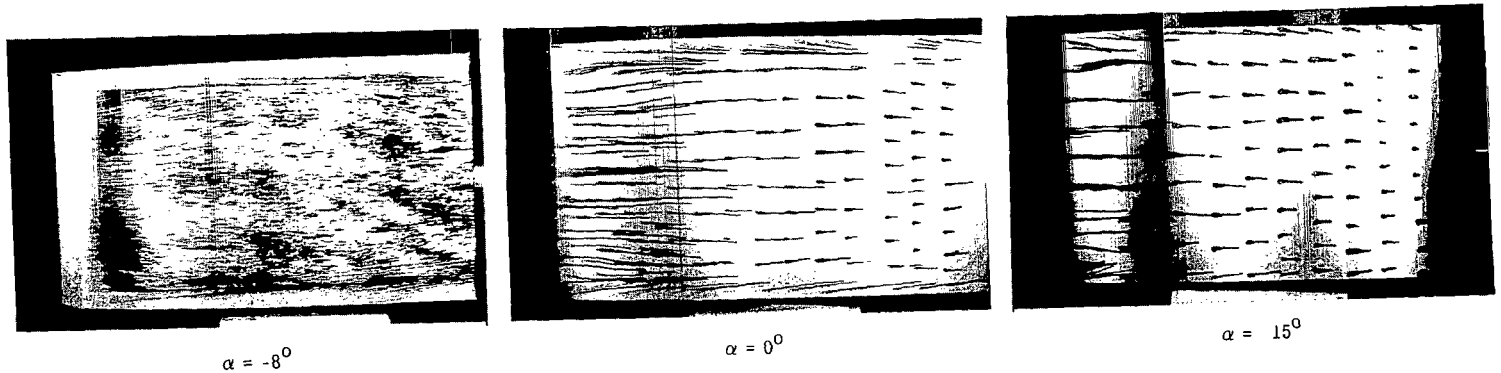

$\alpha = -8^{o}$ $\alpha = 0^{o}$ $\alpha = 15^{o}$

With end plates

L-67-6609

(a) Convex surface.

Figure 7.- Oil-flow photographs at $M = 6.8$ and $R_{\ell} = 7.3 \times 10^{6}$.

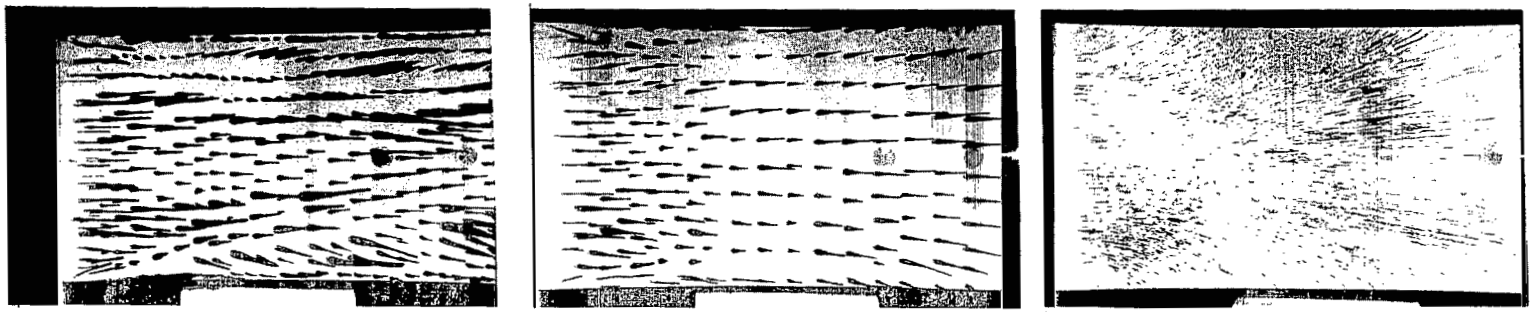

$\alpha = -8^{o}$ $\alpha = 0^{o}$ $\alpha = 15^{o}$

No end plates

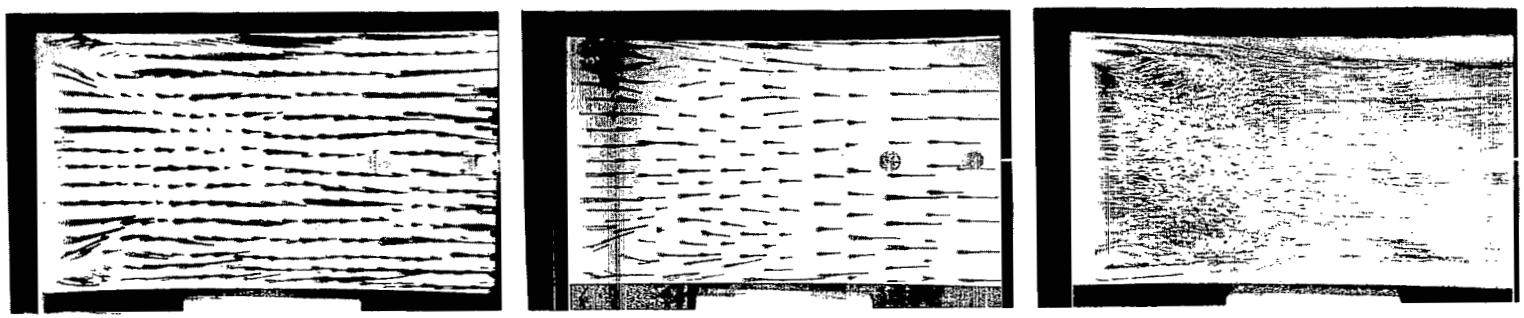

$\alpha = -8^{o}$ $\alpha = 0^{o}$ $\alpha = 15^{o}$

With end plates

(b) Concave surface.

L-67-6610

Figure 7.- Continued.

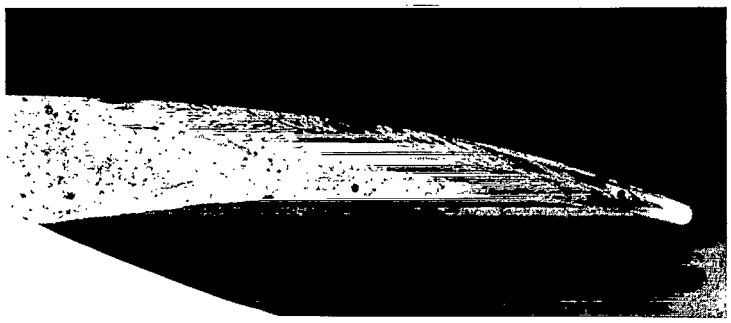

$\alpha = 15^{o}$

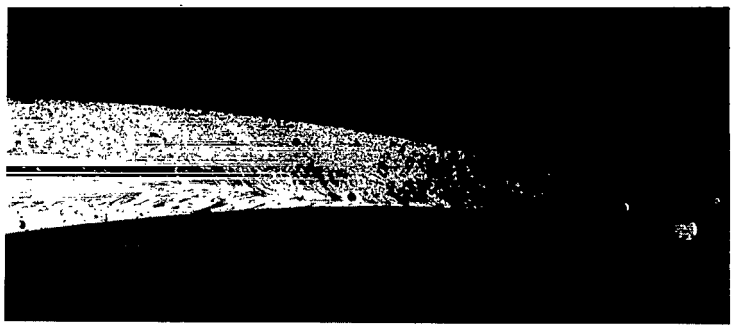

$\alpha = 0^{o}$

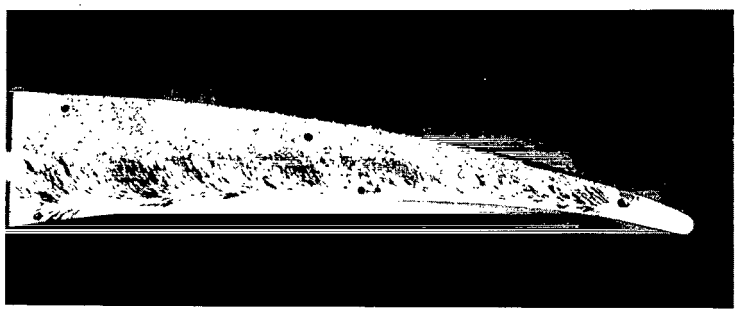

$\alpha = -8^{o}$

(c) Vortex evidence alongside of model. L-67-6611

Figure 7.- Concluded.

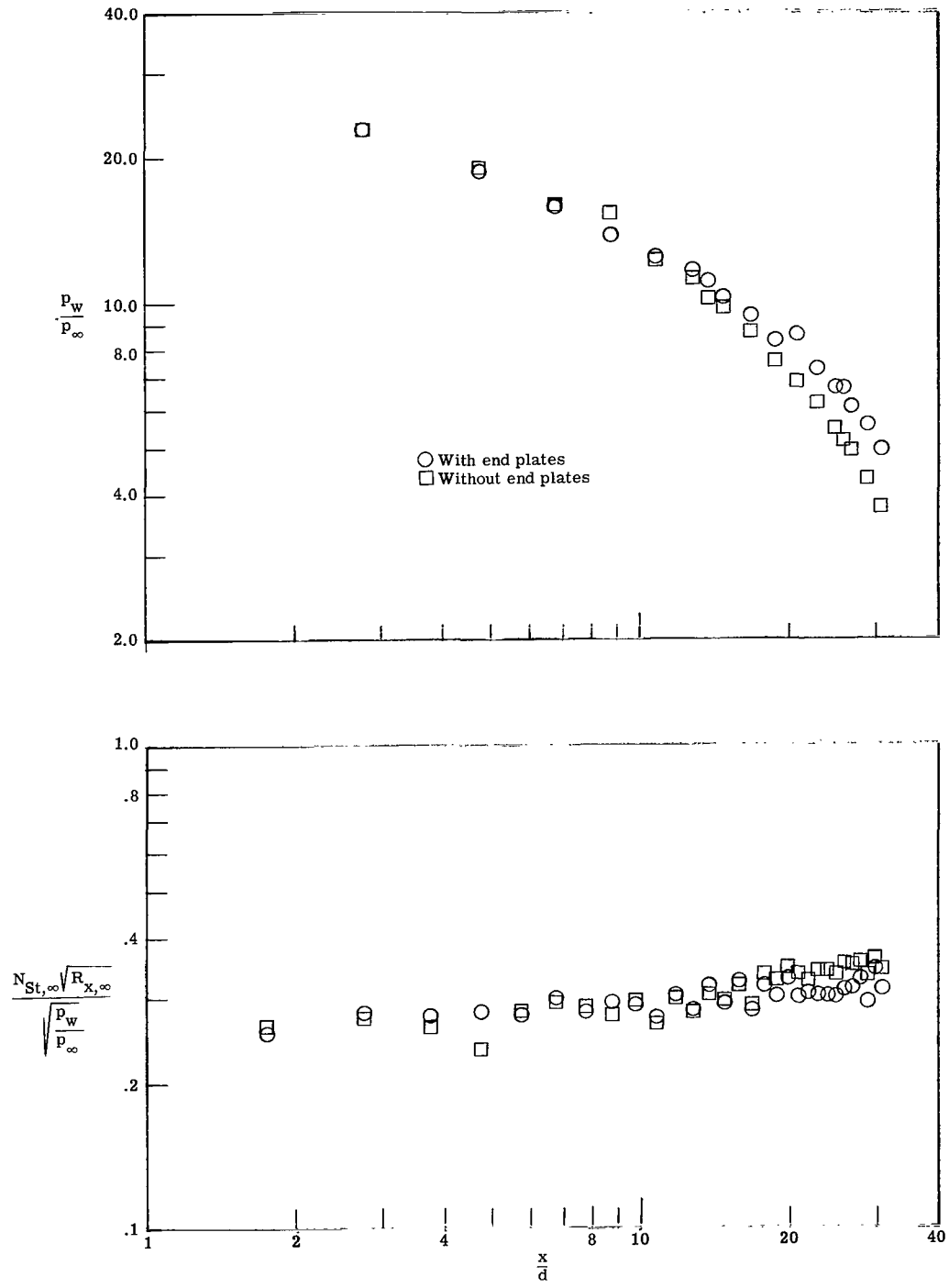

(a) Convex surface; $\alpha = -8^0$.

Figure 8.- Pressure and heat transfer on blunt curved plates with and without end plates at $M = 6.8$ and $R_{l,\infty} = 1.5 \times 10^6$.

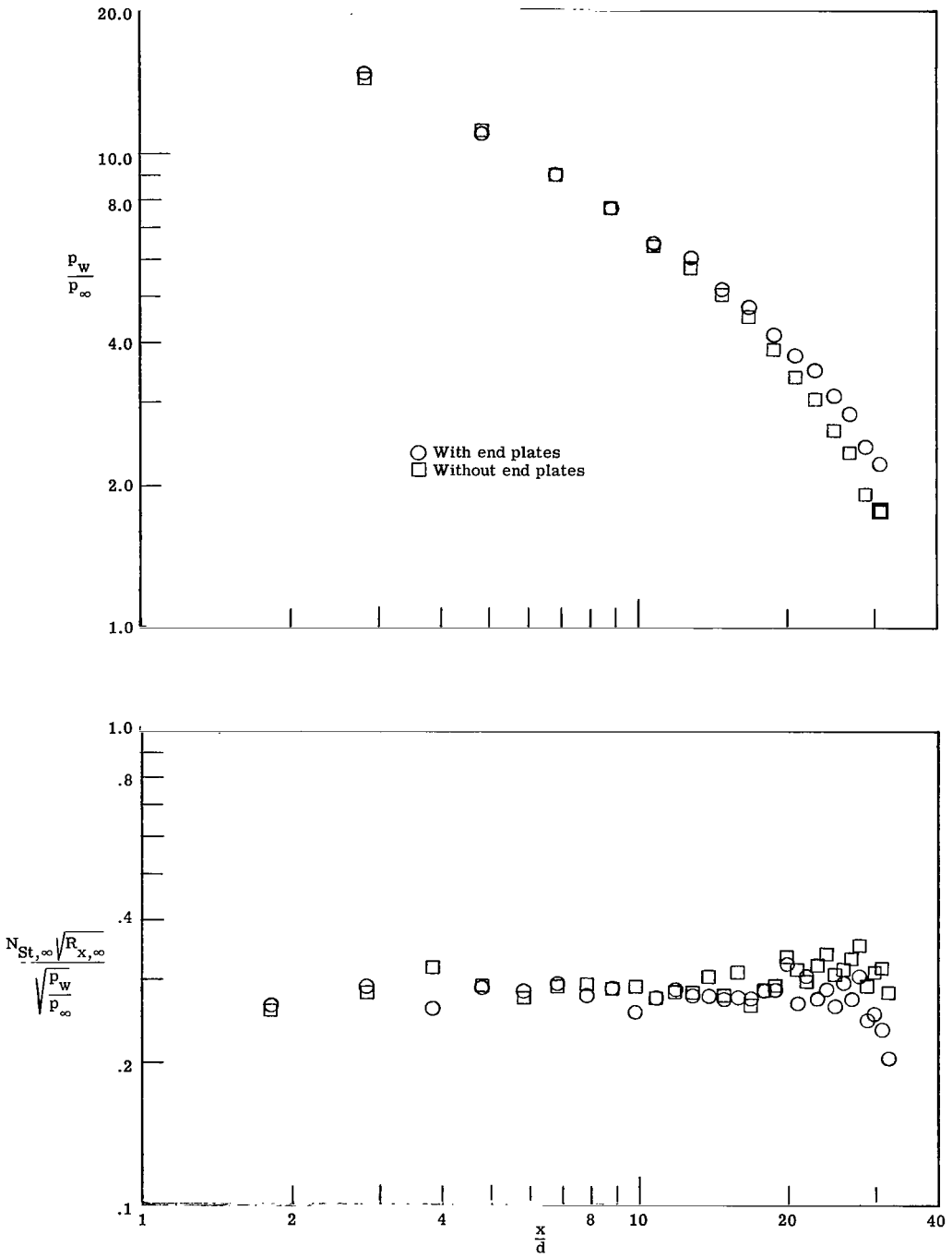

(b) Convex surface; $\alpha = 0^0$.

Figure 8.- Continued.

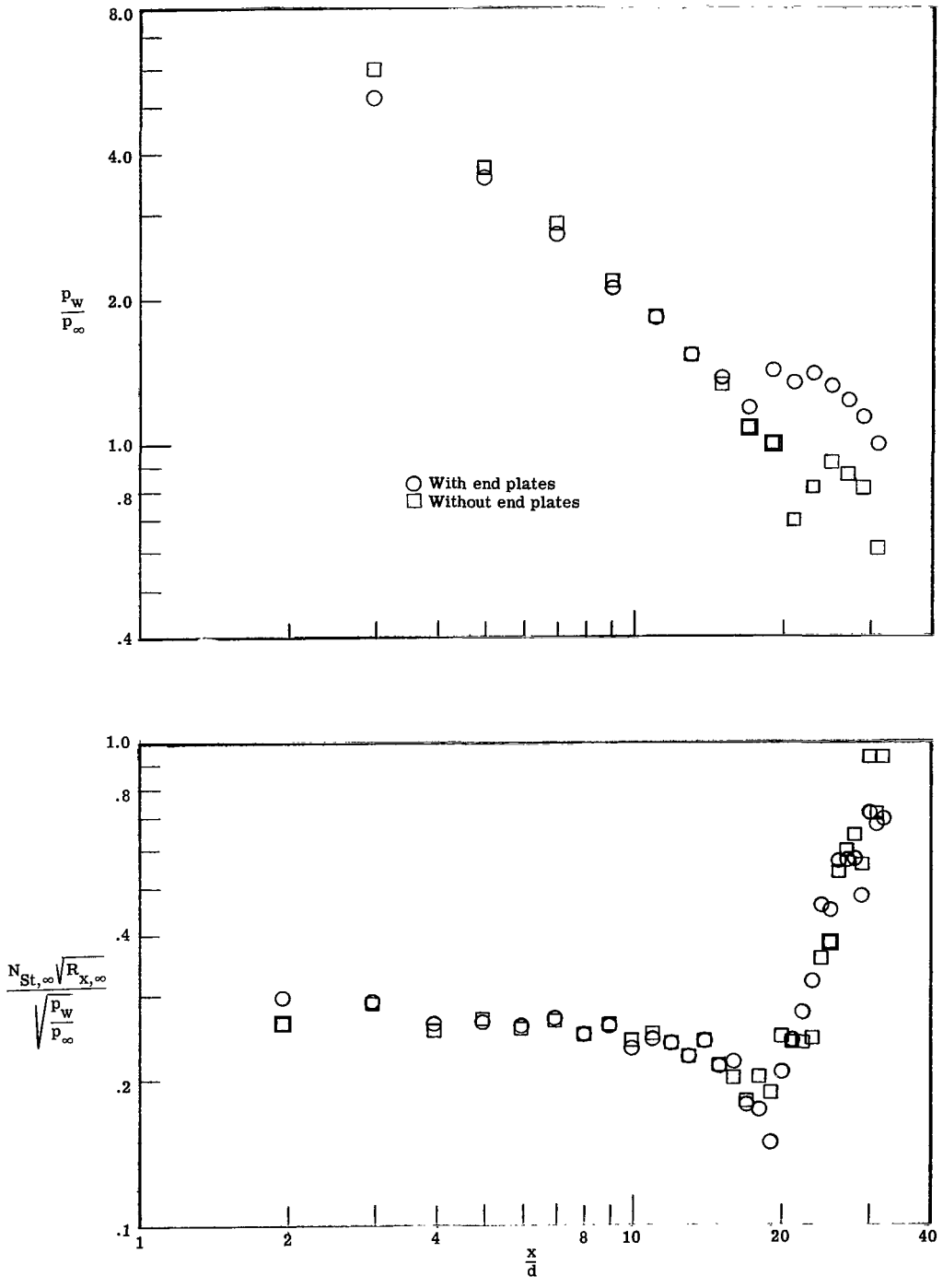

(c) Convex surface; $\alpha = 15^0$.

Figure 8.- Continued.

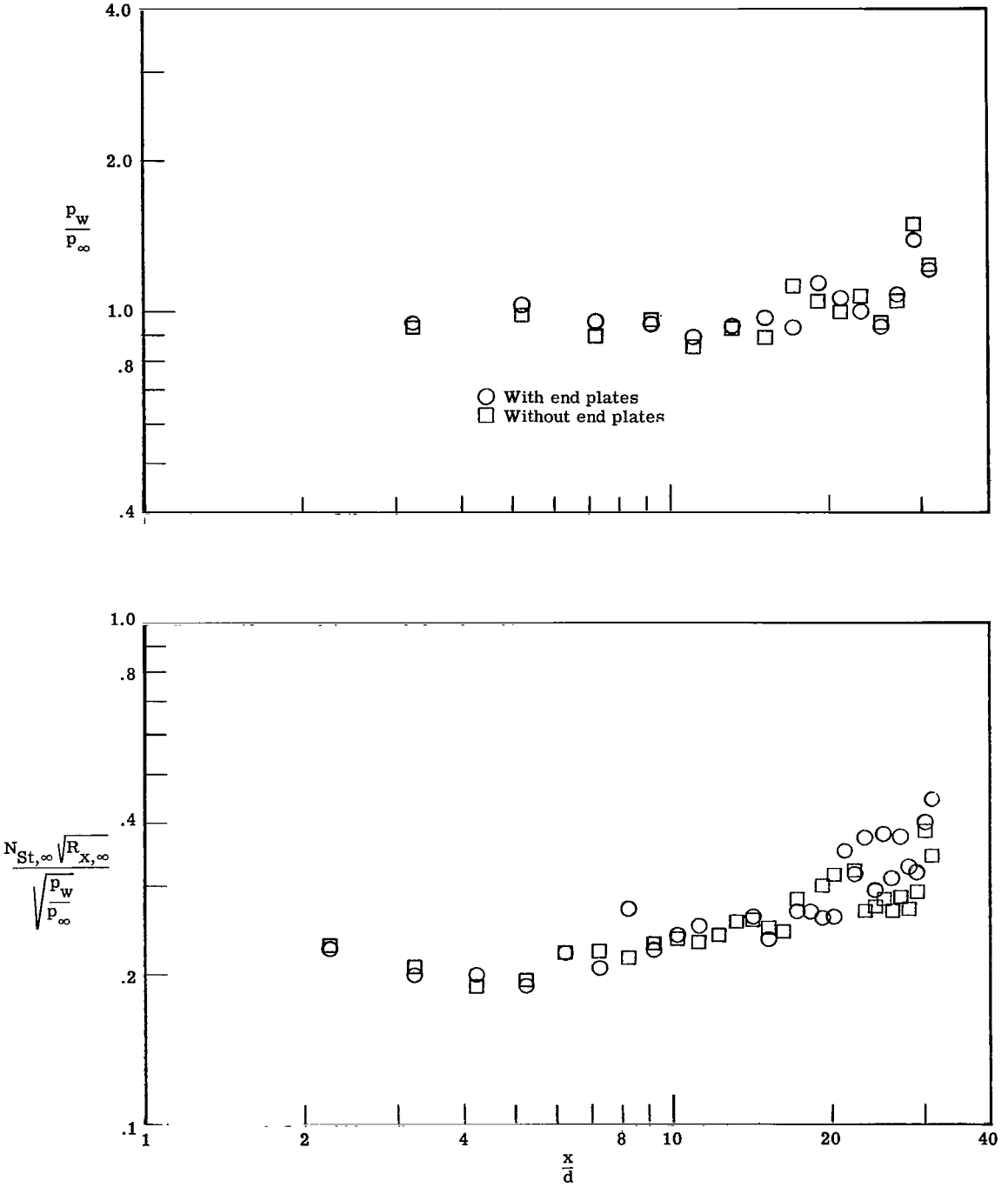

(d) Concave surface; $\alpha = -8^0$.

Figure 8.- Continued.

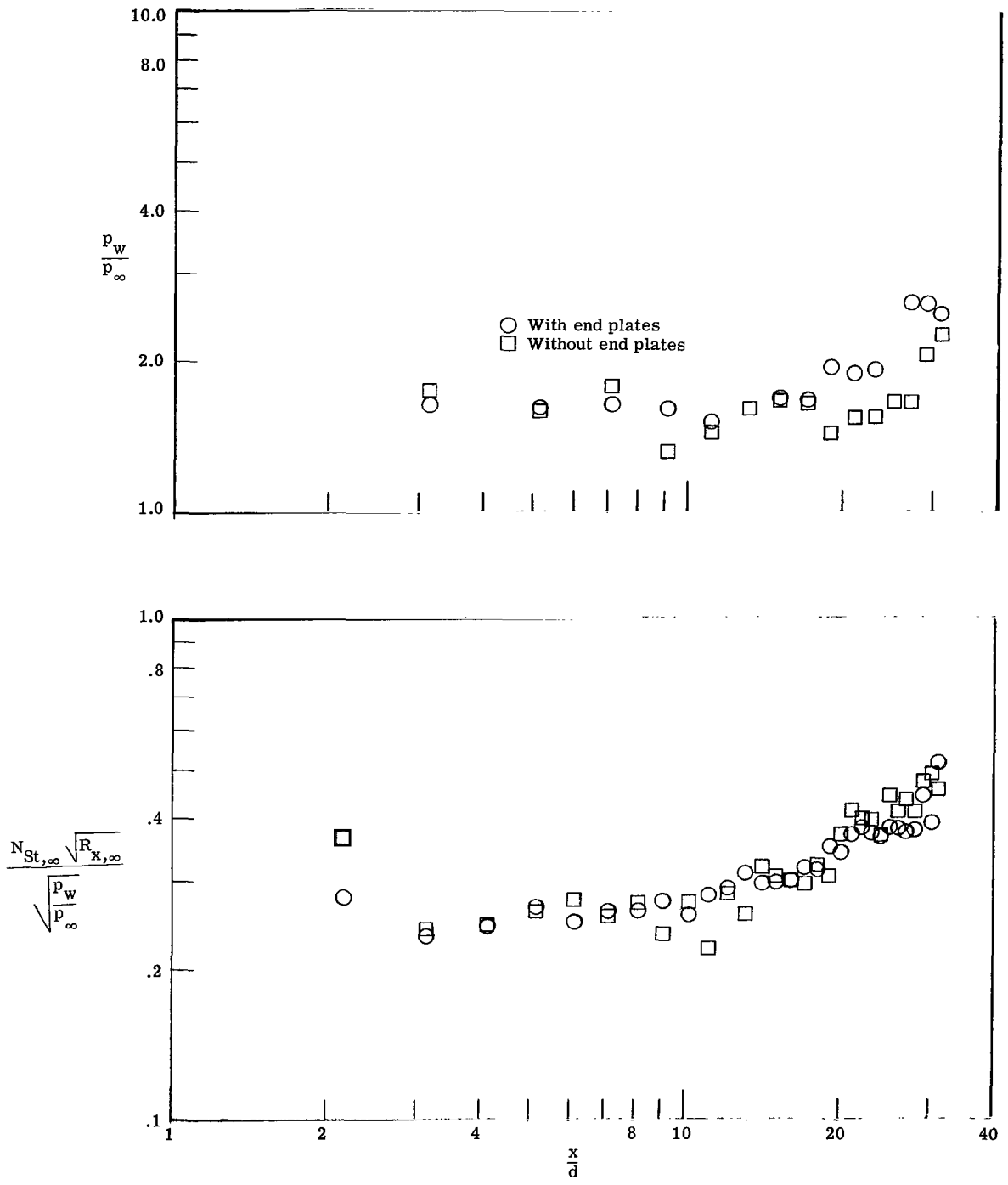

(e) Concave surface; $\alpha = 0^0$.

Figure 8.- Continued.

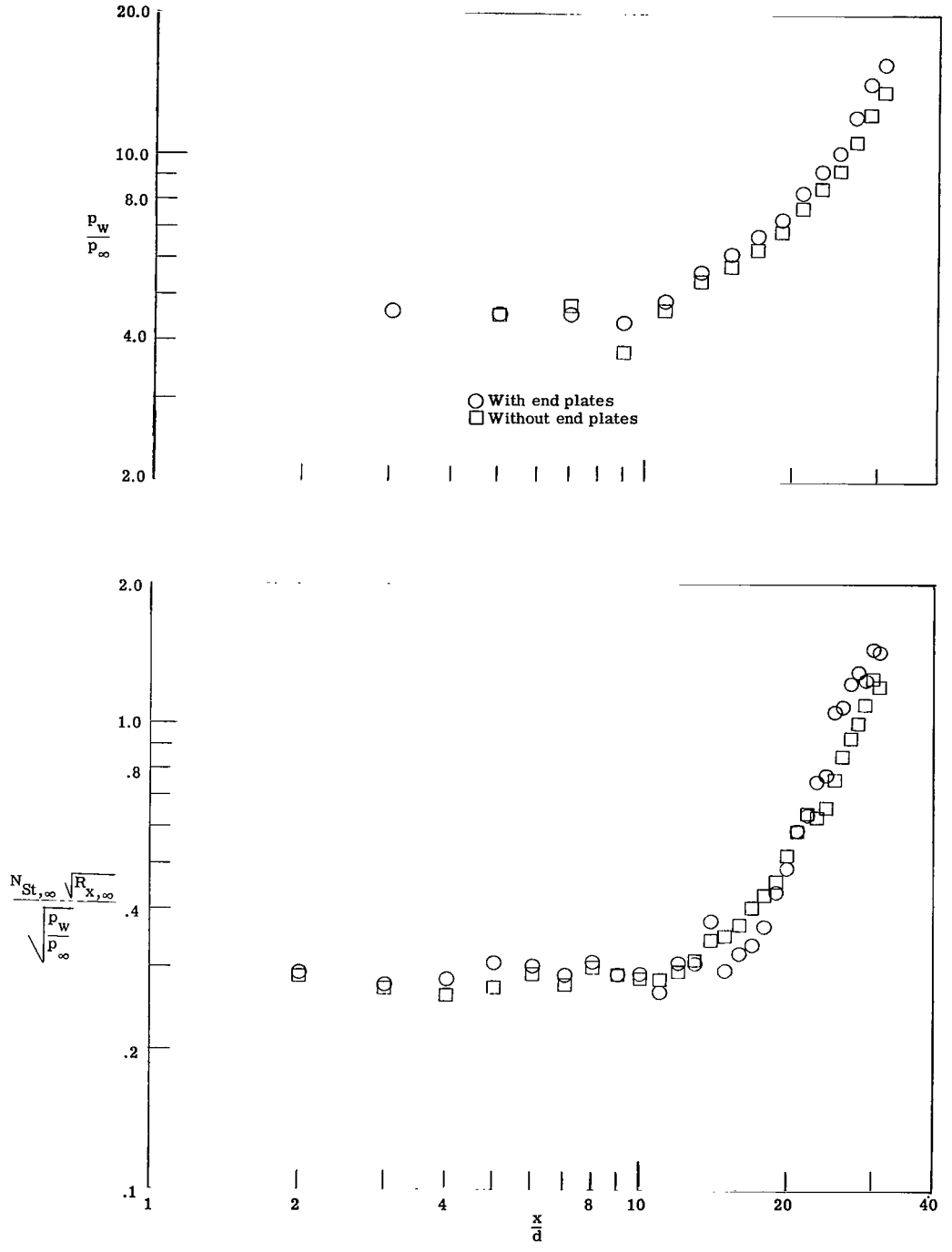

(f) Concave surface; $\alpha = 15^0$.

Figure 8.- Concluded.

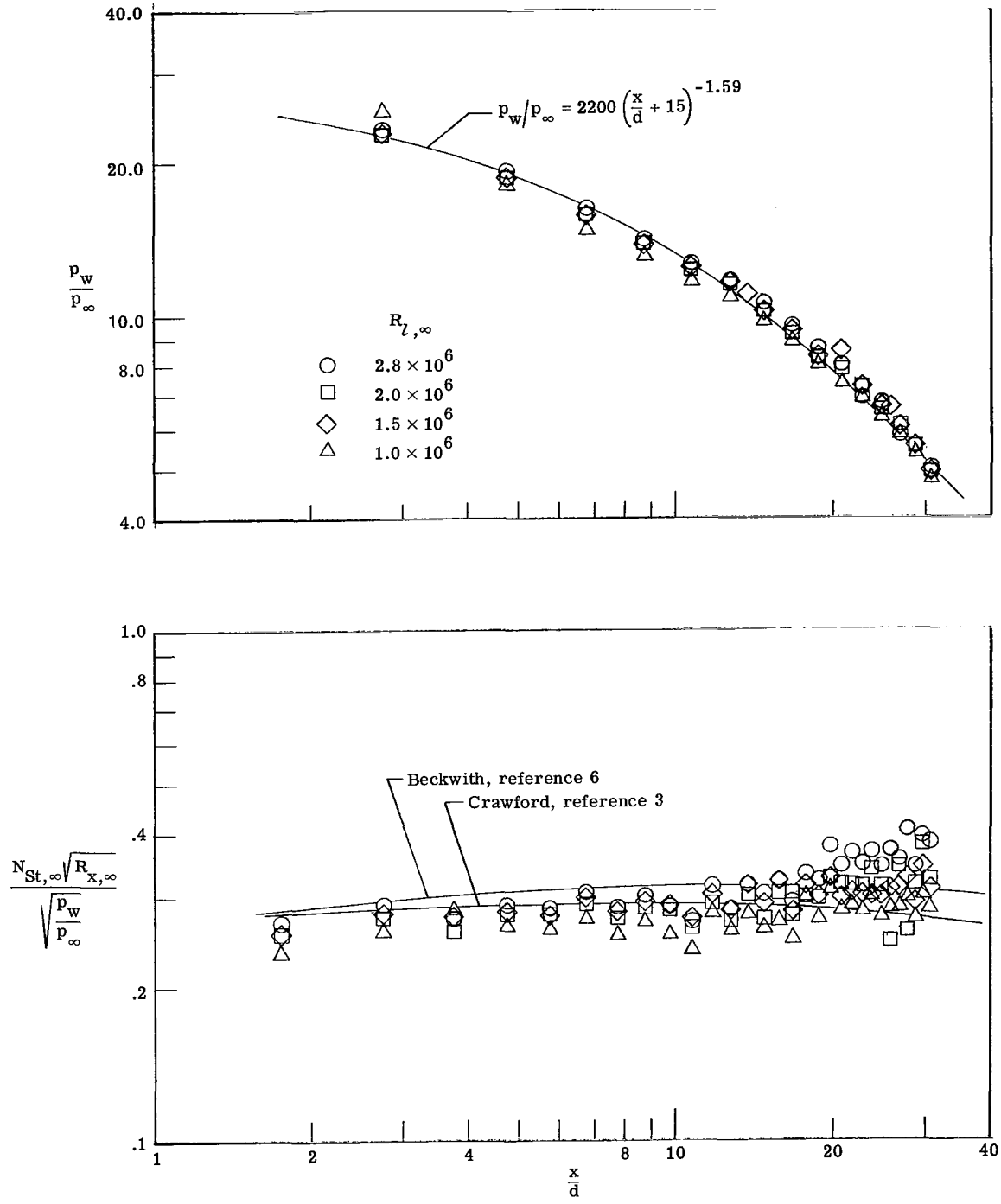

(a) $\alpha = -8^0$; M = 6.8.

Figure 9.- Pressure and heat transfer on convex surface following blunt leading edge.

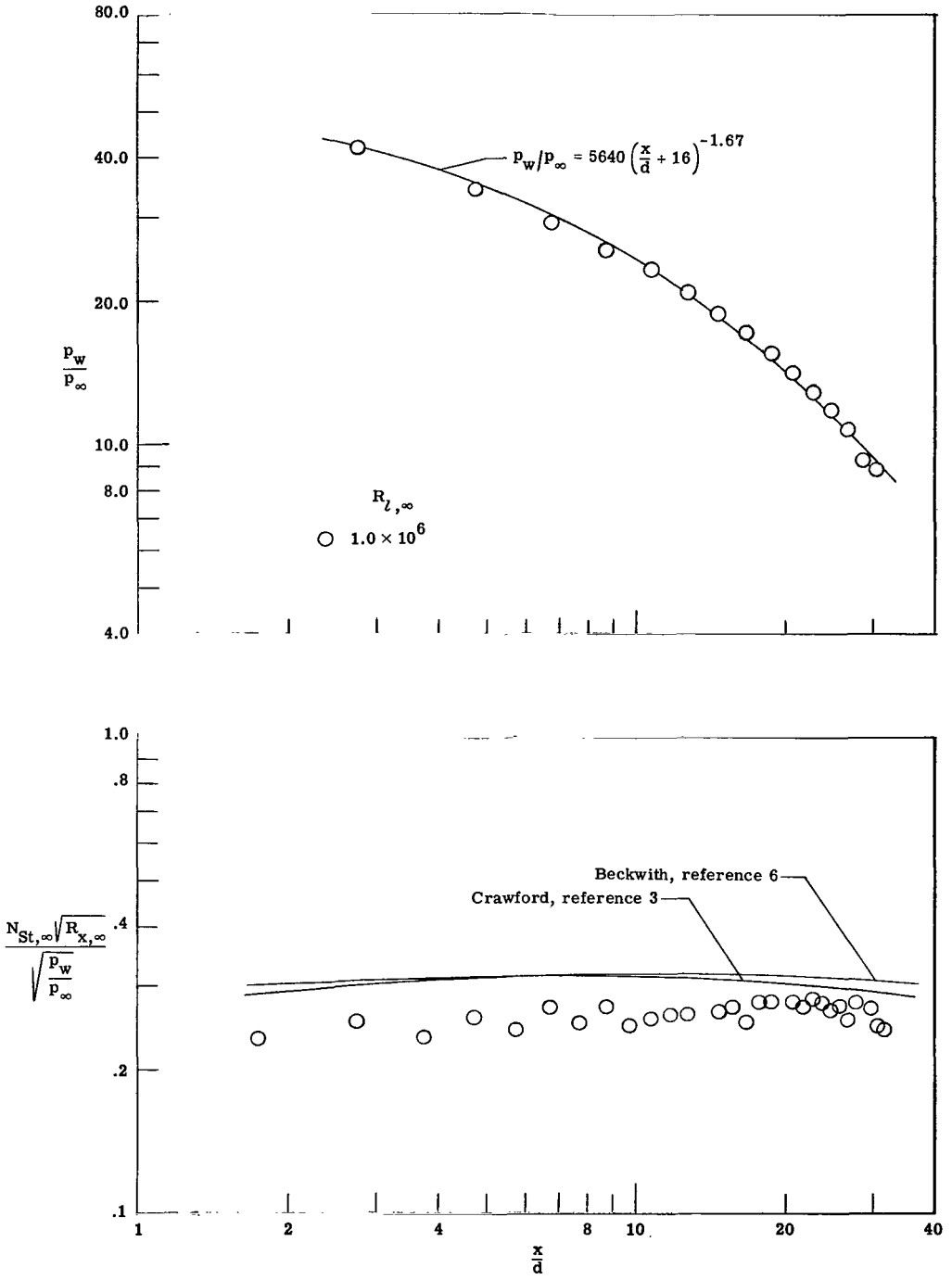

(b) $\alpha = -8^0$; M = 9.6.

Figure 9.- Continued.

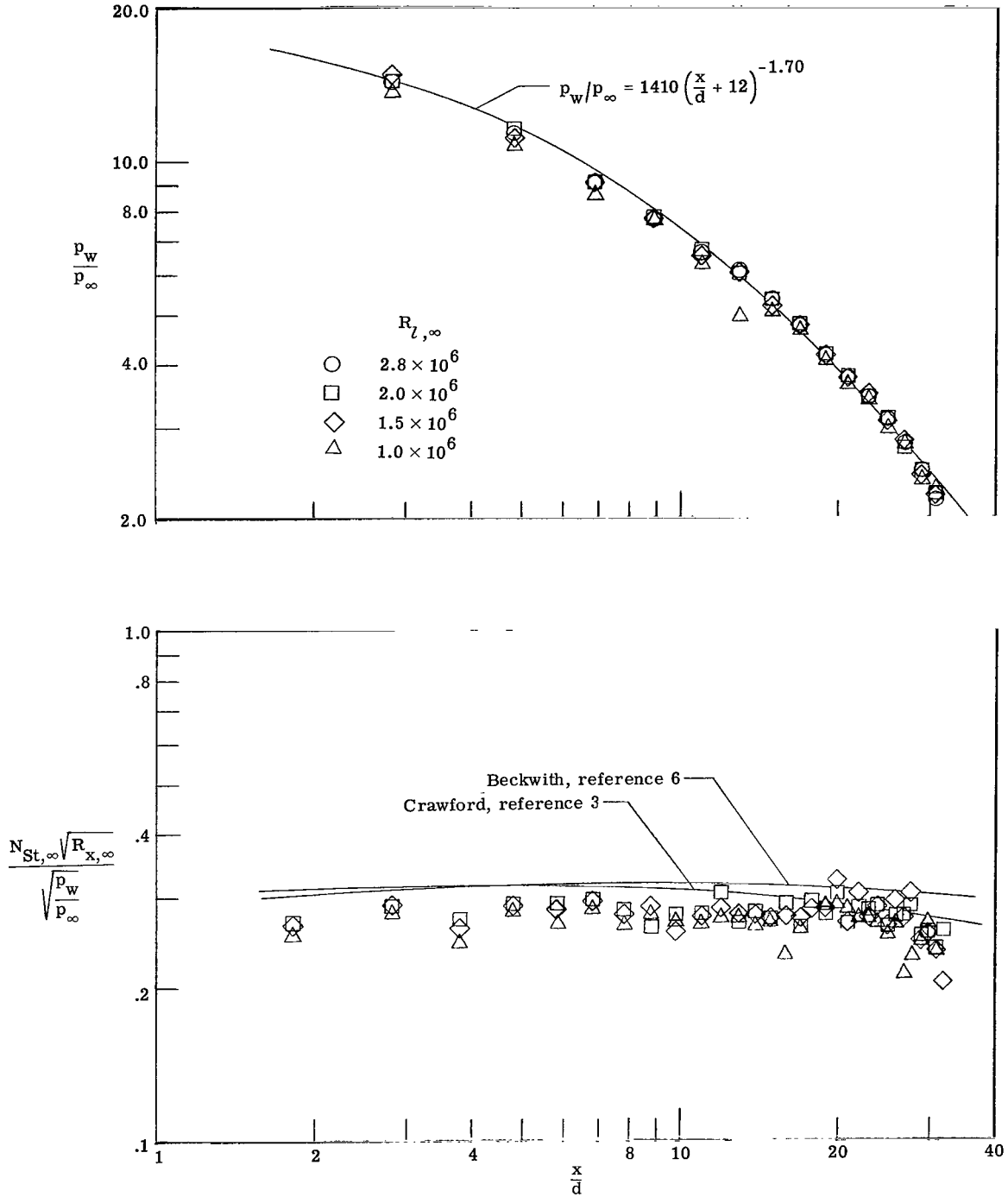

(c) $\alpha = 0^0$; M = 6.8.

Figure 9.- Continued.

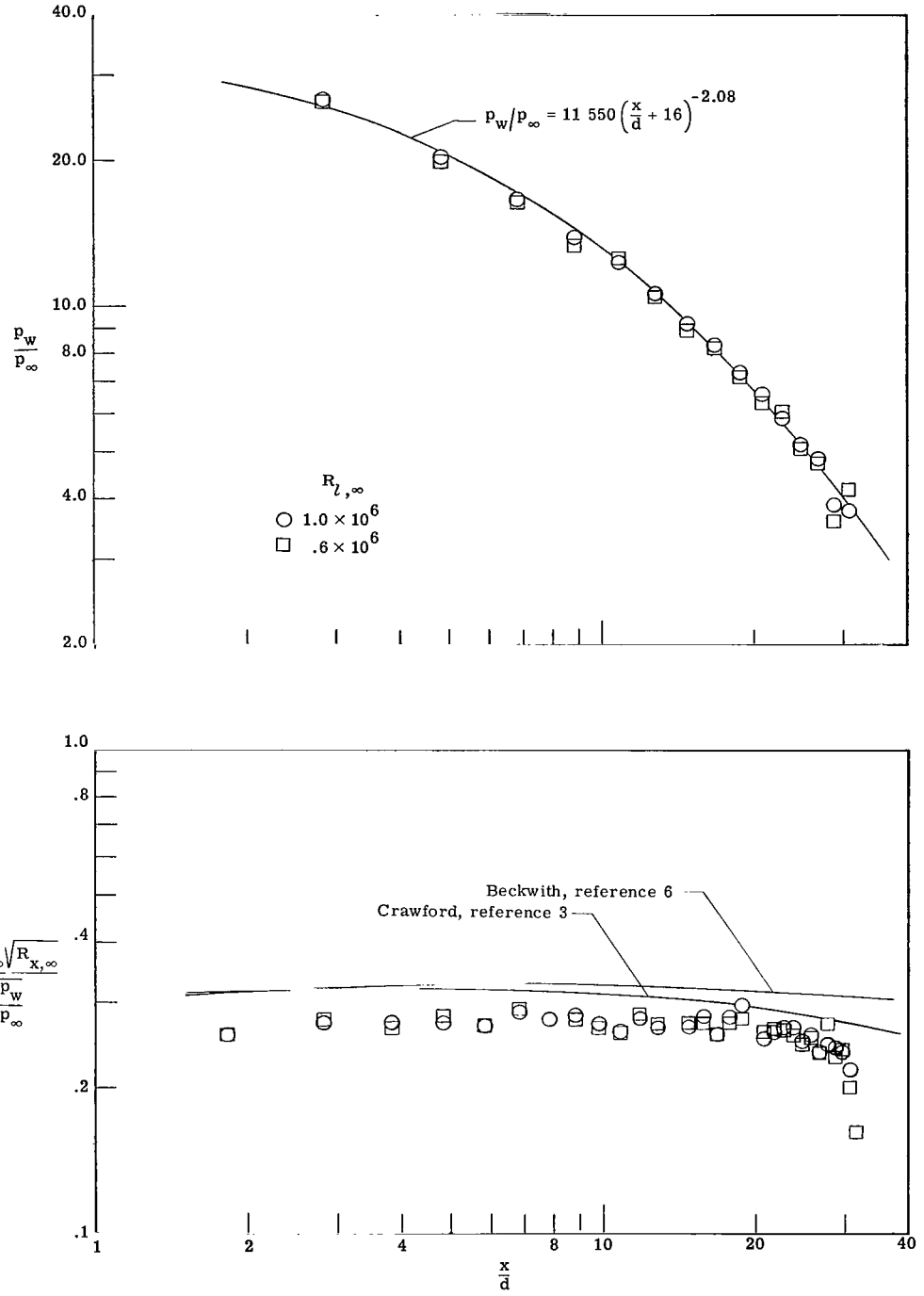

(d) $\alpha = 0^0$; M = 9.6.

Figure 9.- Continued.

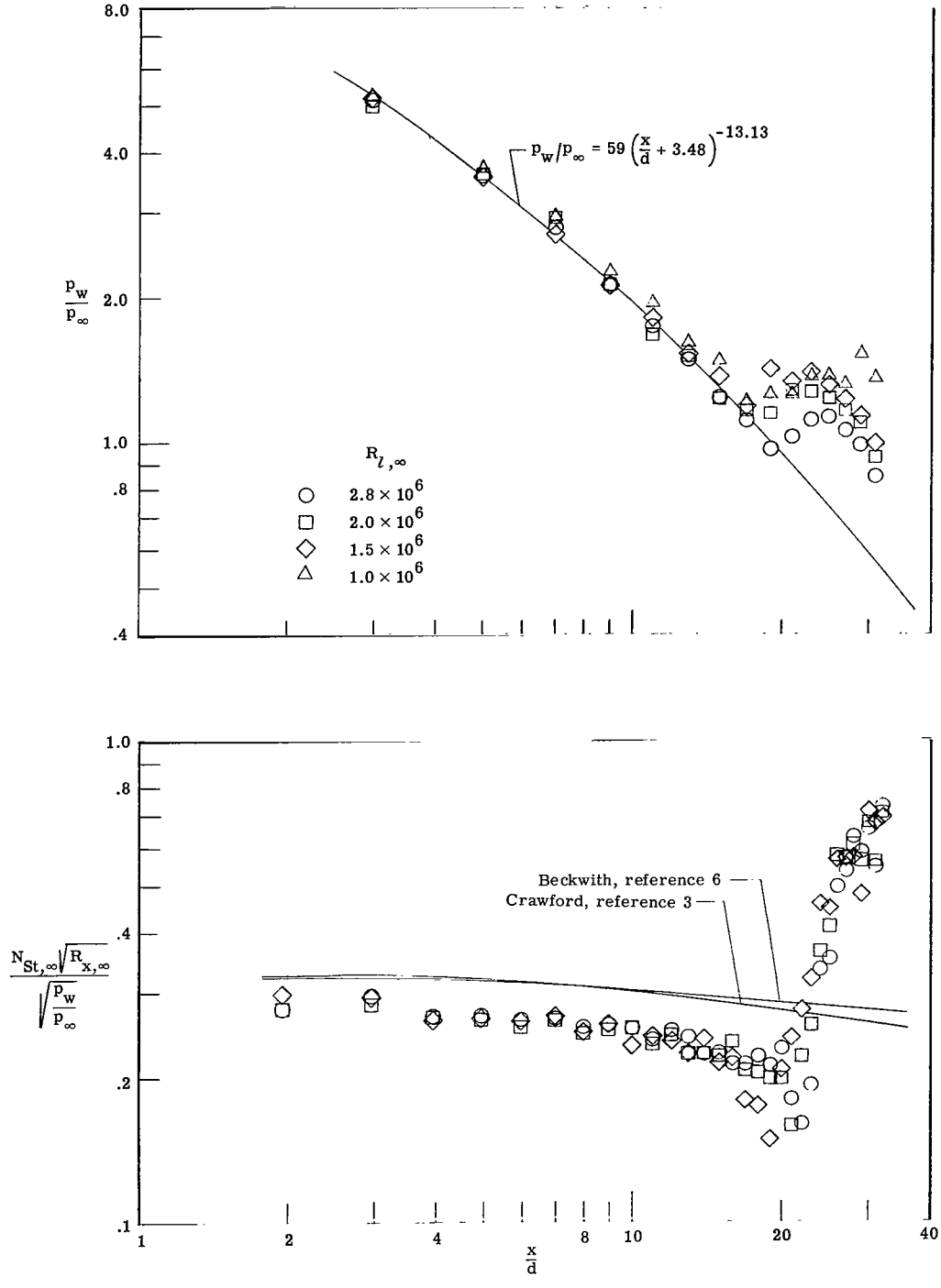

(e) $\alpha = 15^0$; M = 6.8.

Figure 9.- Continued.

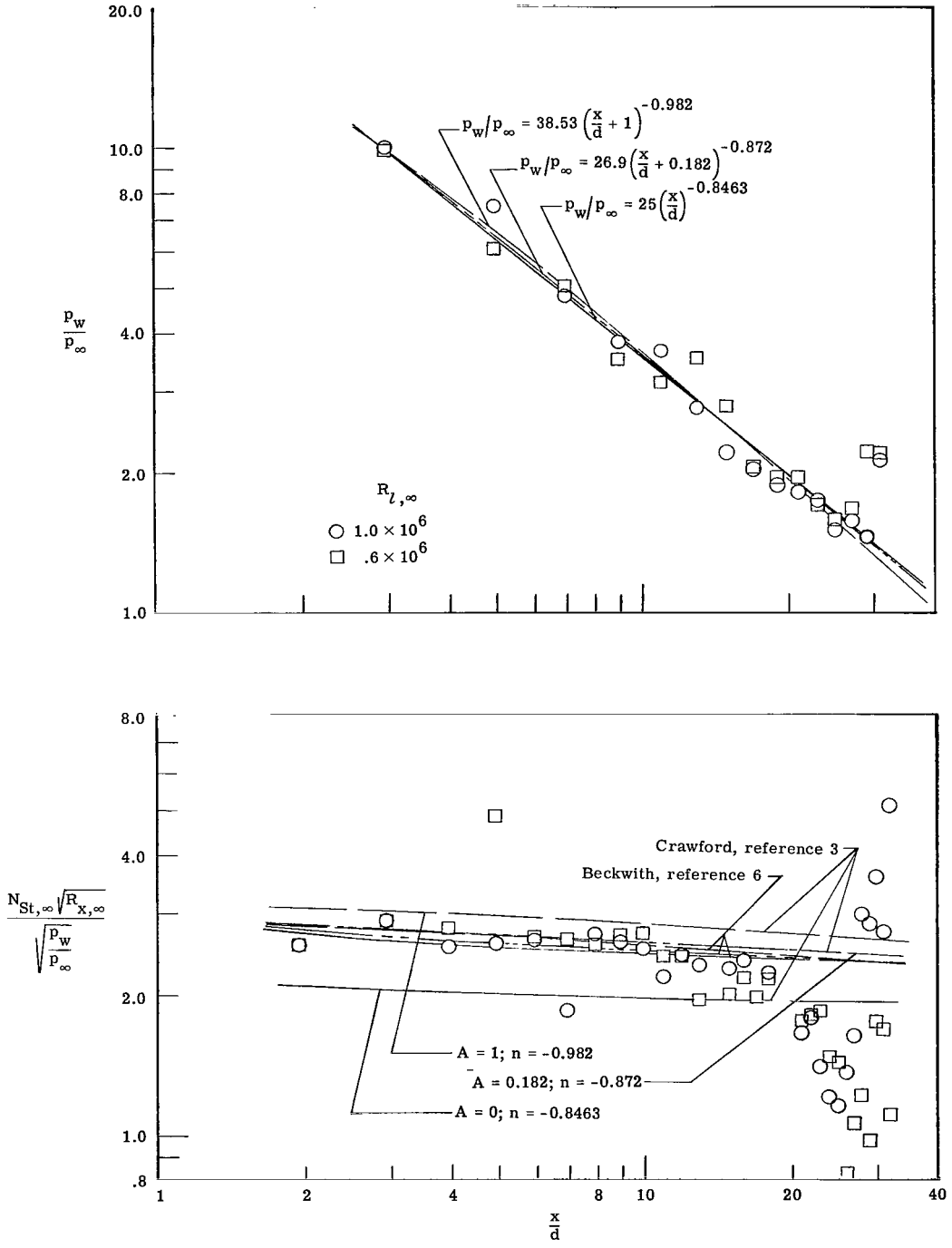

(f) $\alpha = 15^0$; M = 9.6.

Figure 9.- Concluded.

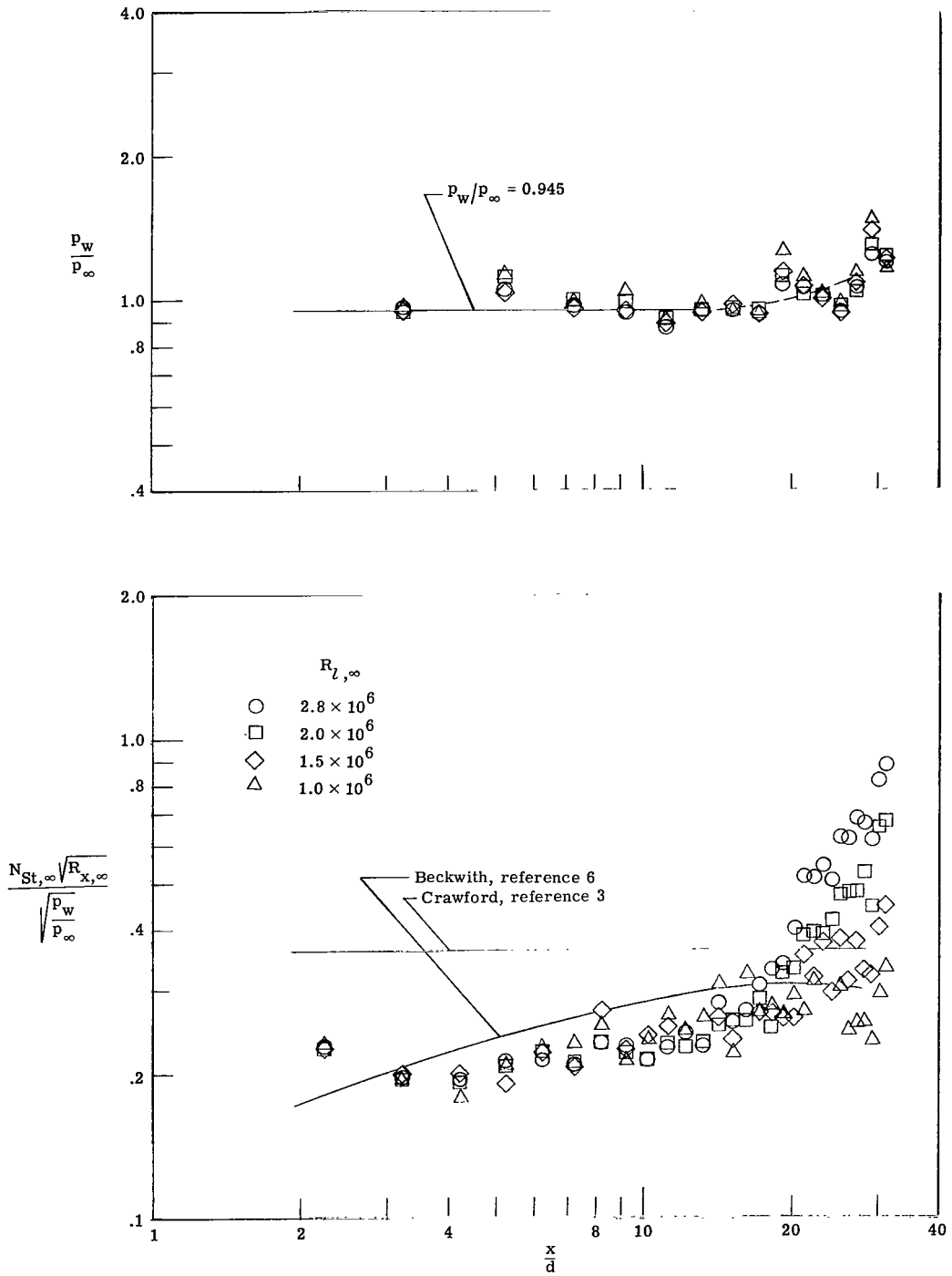

(a) $\alpha = -8^0$; $M = 6.8$.

Figure 10.- Pressure and heat transfer on concave surface following a blunt leading edge.

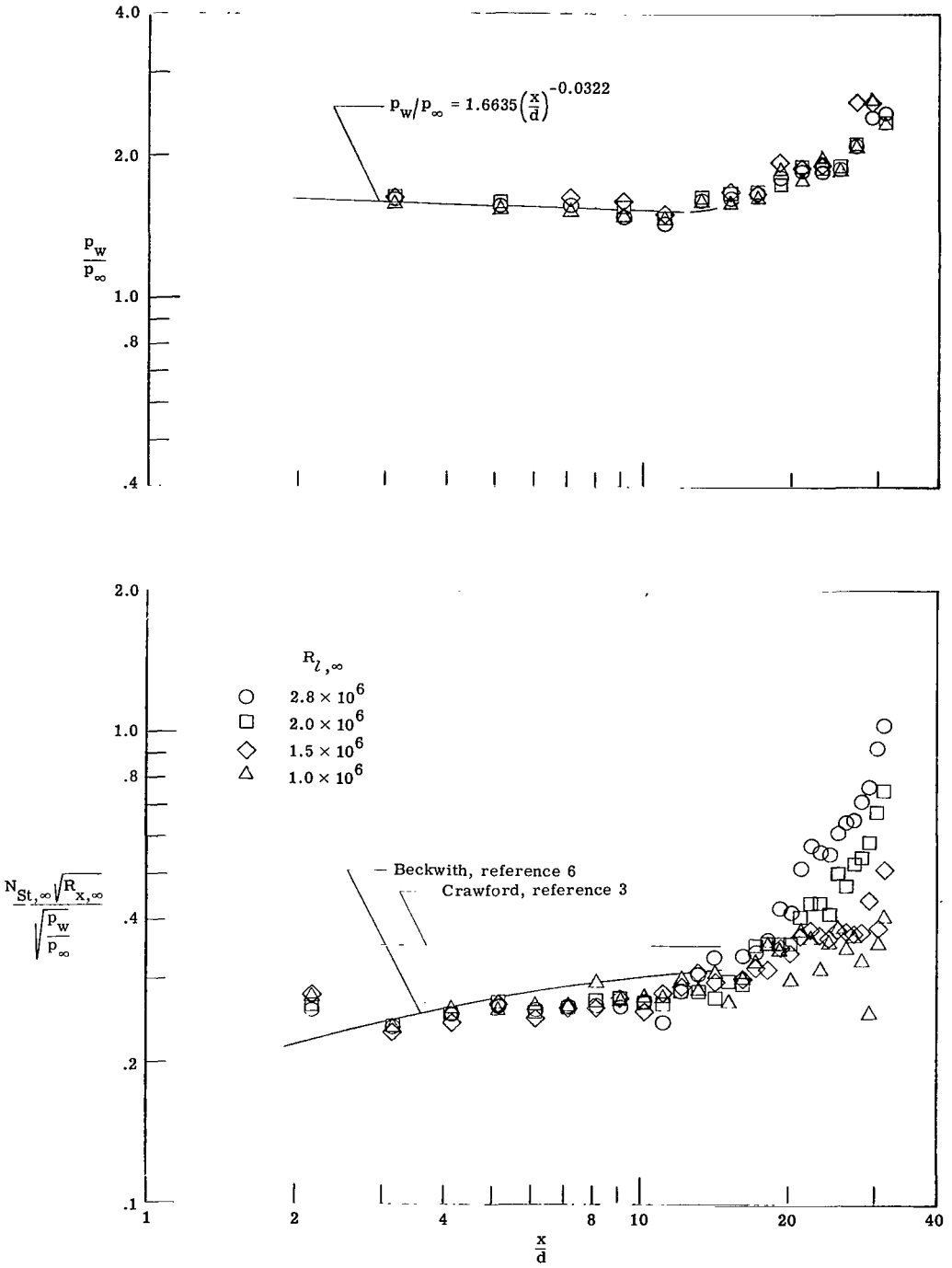

(b) $\alpha = 0^0$; M = 6.8.

Figure 10.- Continued.

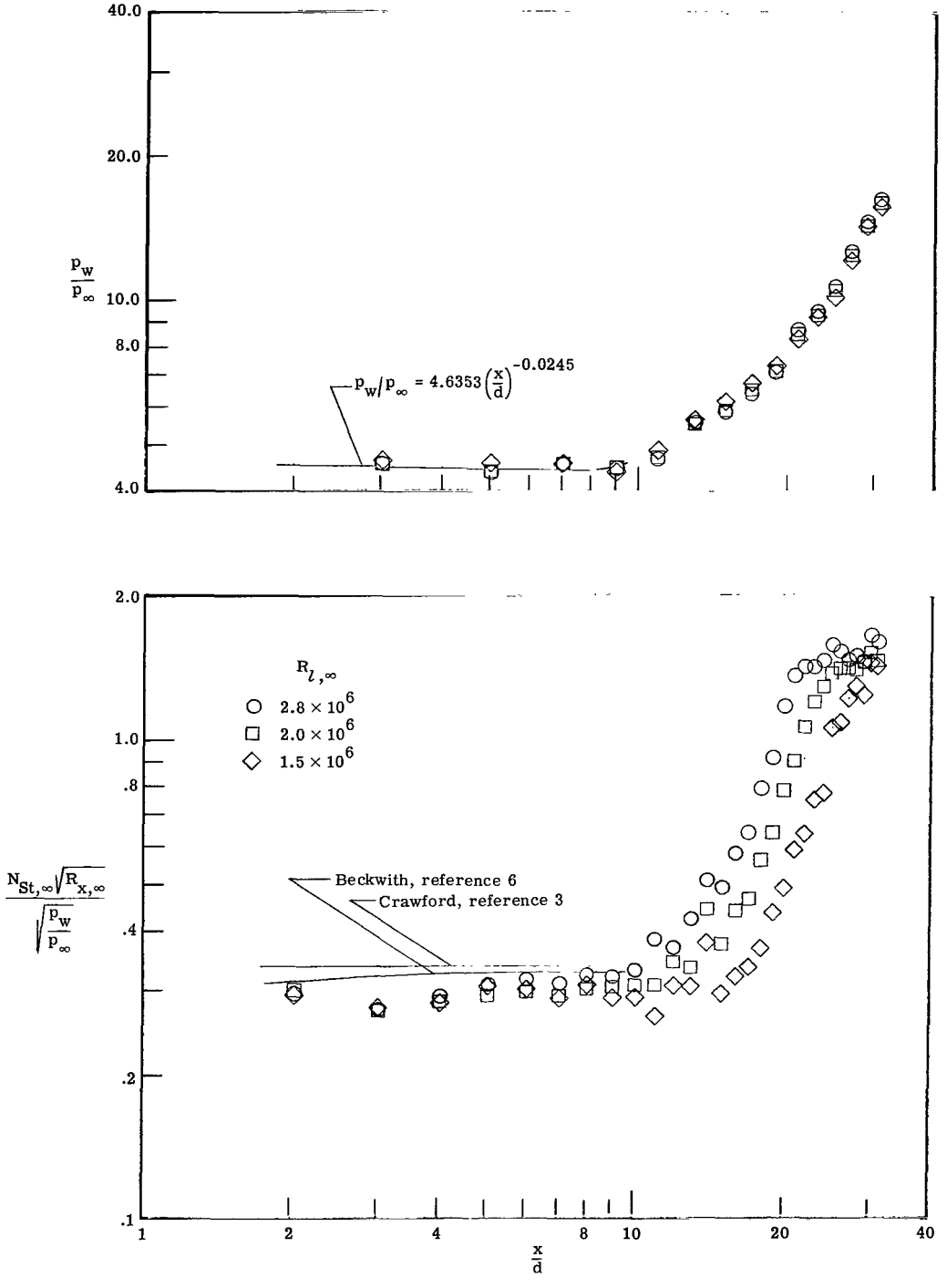

(c) $\alpha = 15^0$; M = 6.8.

Figure 10.- Continued.

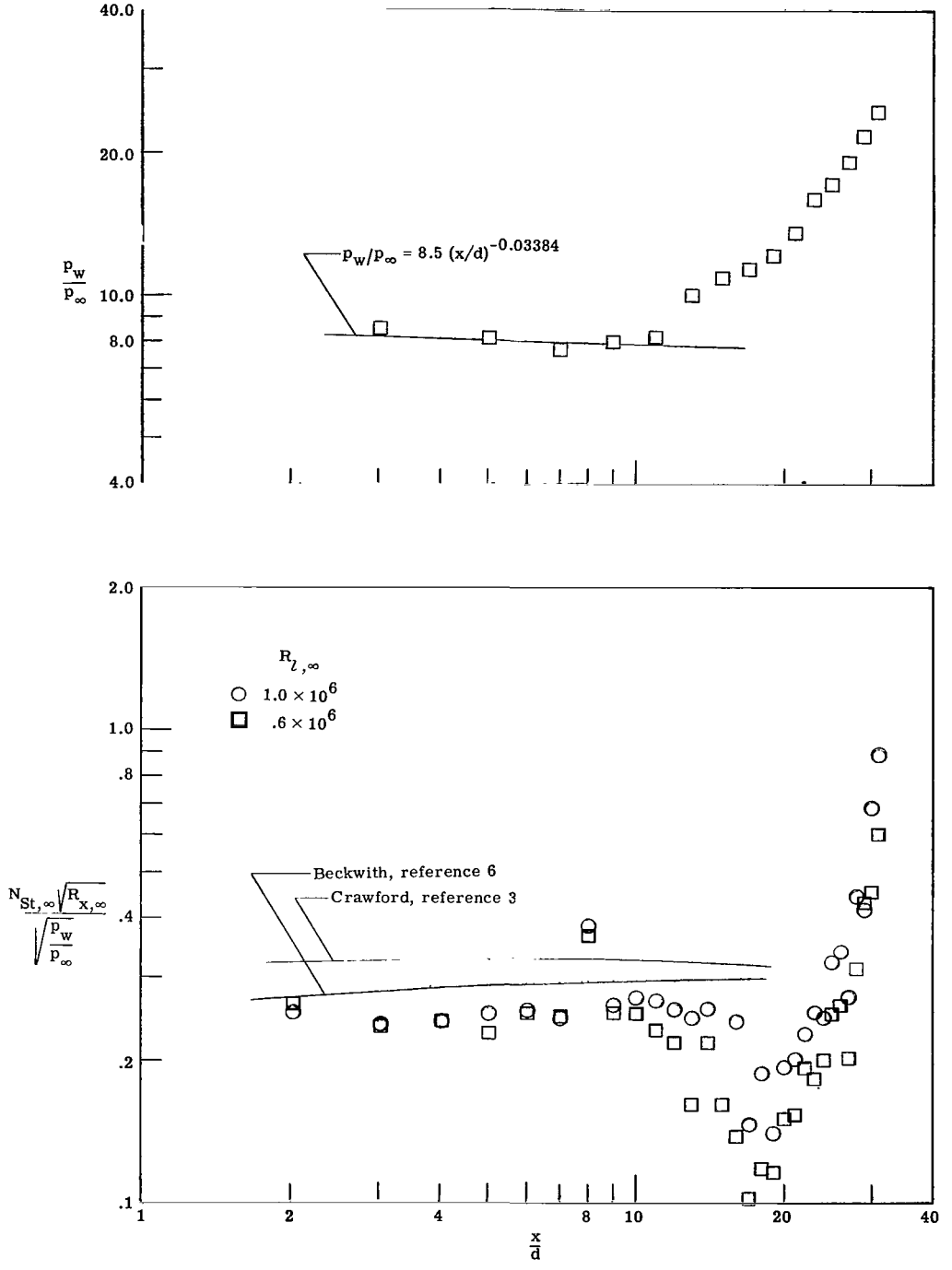

(d) $\alpha = 15^0$; M = 9.6.

Figure 10.- Concluded.

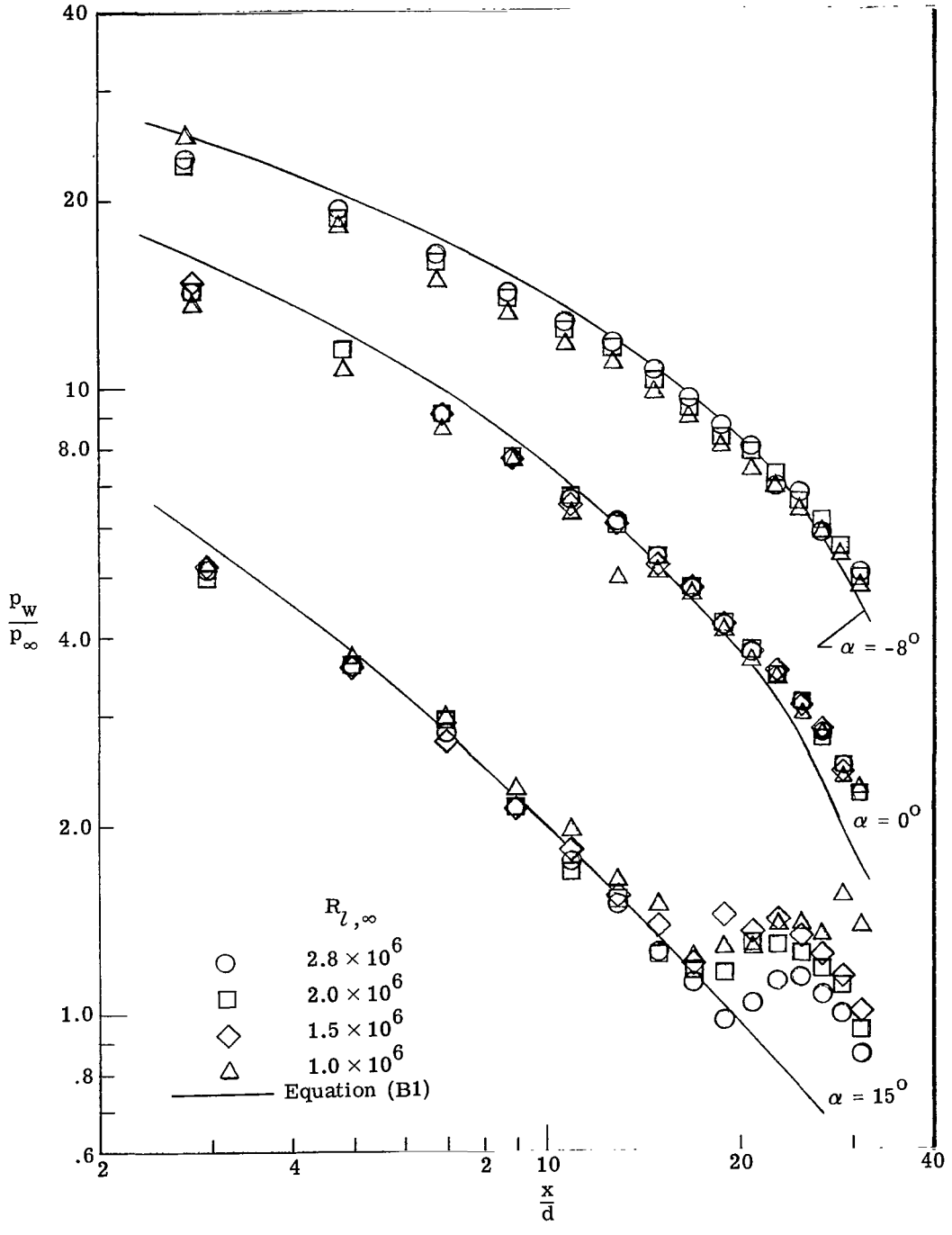

(a) Convex surface; M = 6.8.

Figure 11.- Comparison of simple hypersonic approximations with measured pressure distributions.

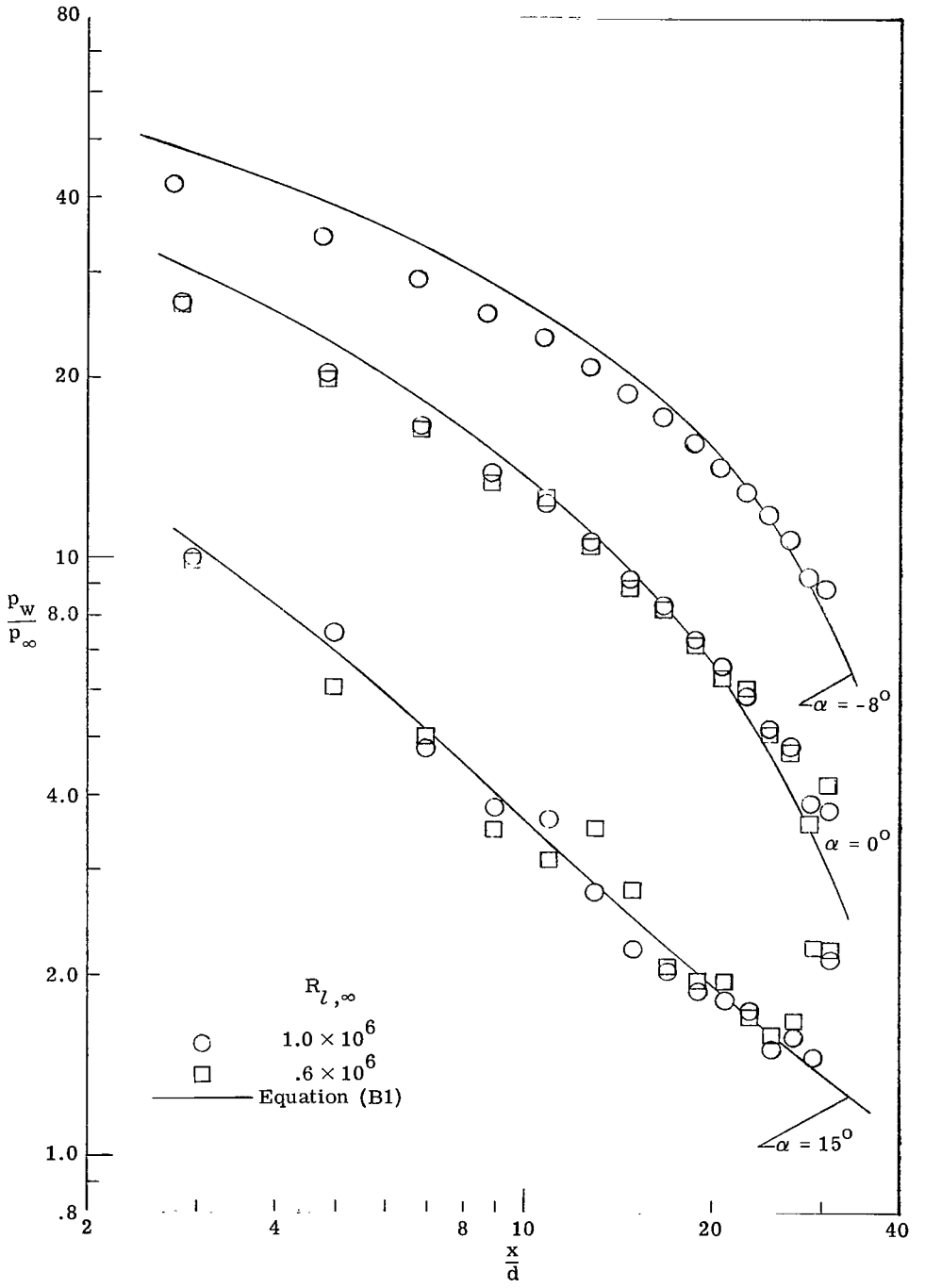

(b) Convex surface; M = 9.6.

Figure 11.- Continued.

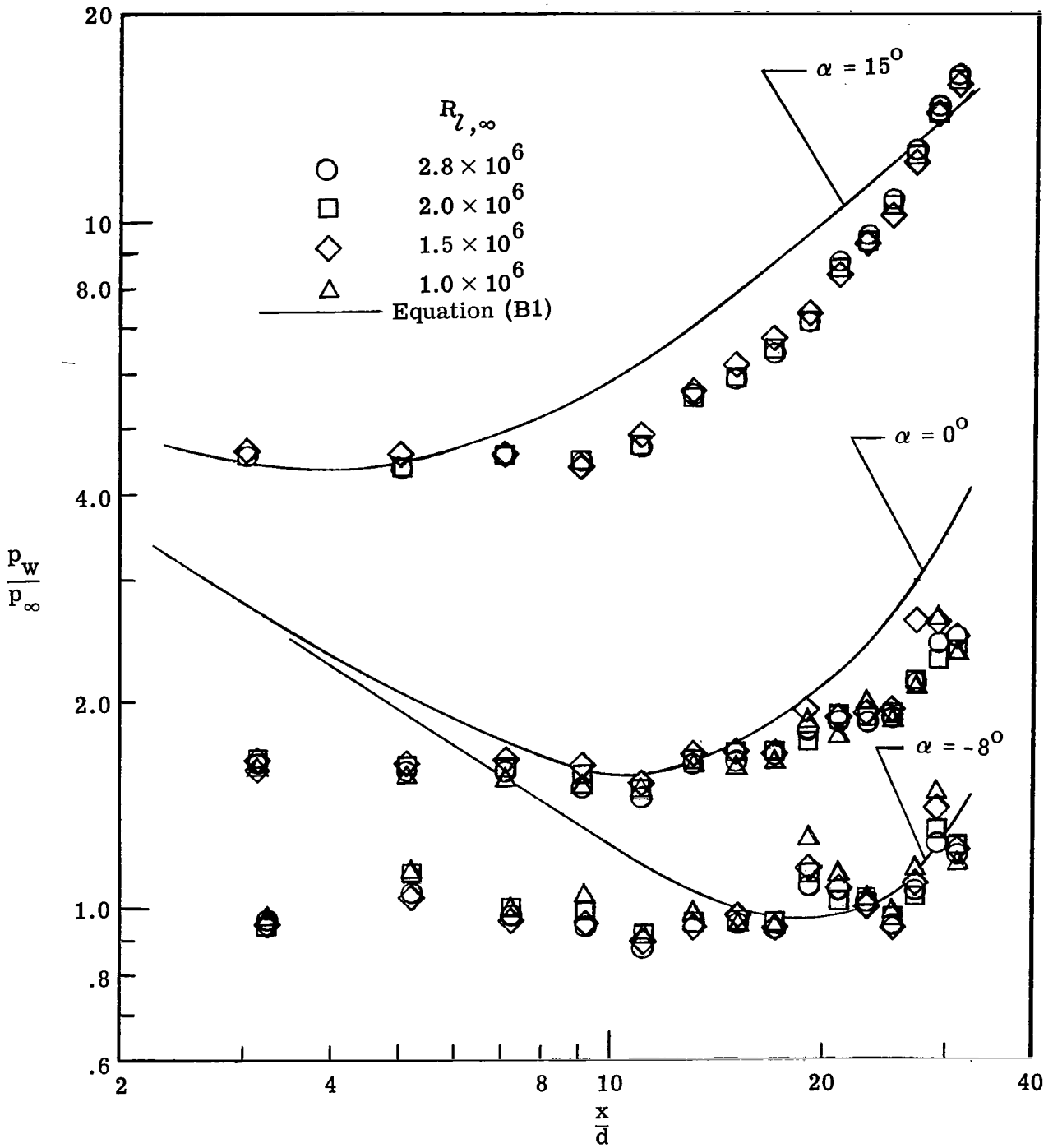

(c) Concave surface; M = 6.8.

Figure 11.- Concluded.

NASA-Langley, 1968 —— 12 L-5353

"The aeronautical and space activities of the United States shall be conducted so as to contribute . . . to the expansion of human knowledge of phenomena in the atmosphere and space. The Administration shall provide for the widest practicable and appropriate dissemination of information concerning its activities and the results thereof."

—NATIONAL AERONAUTICS AND SPACE ACT OF 1958

NASA SCIENTIFIC AND TECHNICAL PUBLICATIONS

TECHNICAL REPORTS: Scientific and technical information considered important, complete, and a lasting contribution to existing knowledge.

TECHNICAL NOTES: Information less broad in scope but nevertheless of importance as a contribution to existing knowledge.

TECHNICAL MEMORANDUMS: Information receiving limited distribution because of preliminary data, security classification, or other reasons.

CONTRACTOR REPORTS: Scientific and technical information generated under a NASA contract or grant and considered an important contribution to existing knowledge.

TECHNICAL TRANSLATIONS: Information published in a foreign language considered to merit NASA distribution in English.

SPECIAL PUBLICATIONS: Information derived from or of value to NASA activities. Publications include conference proceedings, monographs, data compilations, handbooks, sourcebooks, and special bibliographies.

TECHNOLOGY UTILIZATION PUBLICATIONS: Information on technology used by NASA that may be of particular interest in commercial and other non-aerospace applications. Publications include Tech Briefs, Technology Utilization Reports and Notes, and Technology Surveys.

Details on the availability of these publications may be obtained from:

SCIENTIFIC AND TECHNICAL INFORMATION DIVISION

NATIONAL AERONAUTICS AND SPACE ADMINISTRATION

Washington, D.C. 20546